



**Politecnico  
di Torino**

Politecnico di Torino

Department of Applied Science and Technology

Master's Degree in Nanotechnologies for ICTs

a.a. 22/23

# Metal sensing through fluorescence quenching: the role of carbon quantum dots as fluorescent probes

Supervisors:

Professor Alberto Tagliaferro

Dr. Mattia Bartoli

Candidate:

Marco Giuseppe Giordano

*To Mariuzza and her pomegranates,*

*“H: Tu sei chi scegli e cerchi di essere.*

*G: Superman.”*

*- Il gigante di ferro, 1999*

# Table of contents

1	Introduction.....	5
1.1	Carbon Dots: What they are.....	5
1.1.1	Hints on Discovery of Carbon Dots.....	6
1.1.2	Synthesis of Carbon Dots.....	6
1.1.3	Properties of Carbon Dots .....	7
1.2	Metal Sensing .....	15
2	Aim of the work .....	17
3	Materials and methods .....	17
3.1	Materials: Reagents and instrumentation.....	17
3.2	Methods .....	17
3.2.1	Synthesis of CDs.....	17
3.2.2	Metal Conjugations .....	17
3.2.3	Spectroscopic characterizations.....	18
3.2.3.1	FTIR analysis .....	18
3.2.3.2	UV-Vis analysis .....	19
3.2.3.3	Fluorescence analysis.....	19
3.2.3.4	Raman analysis.....	20
4	Results .....	21
4.1	Synthesis Process.....	21
4.2	Spectroscopic Characterizations .....	24
4.2.1	FTIR Analysis .....	24
4.2.2	UV-Vis analysis.....	25
4.2.3	Fluorescence analysis .....	26
4.2.4	Raman Analysis.....	31
4.3	Metal Sensing .....	33
4.3.1	Cr(III) Sensing.....	33
4.3.2	Fe(III) Sensing.....	35
4.3.3	Quenching Comparison .....	37
5	Conclusions.....	42

## Abstract

Carbon dots are a class of carbon nanoparticles which possess interesting properties such as high fluorescence, high solubility and size in the nanometre range. This thesis work focused on the role of carbon dots as fluorescent probes for harmful metals sensing through the phenomenon of fluorescence quenching, in which the intensity of the fluorescence emission of the carbon dots is reduced following a bonding with a metal particle. For this application, glucose-based carbon dots were synthesised through hydrothermal method in an autoclave at 200°C, followed by purification by dialysis with the use of a 5kDa cut-off membrane, lasting 72h. Lastly, the resulting nanoparticles were thermally treated in an oven at 60°C for several days. Characterization was done with several methods, namely FTIR, Raman spectroscopy, UV-Vis spectroscopy and fluorescence spectroscopy. The first four were used to determine the quality and chemical identity of the carbon dots, while the last one was adopted to study the fluorescent behaviour both for a solution containing only the carbon dots and for a solution in which metal particles were also inserted, and quenching was observed. The first solution was comprised of 0.7mg/mL of carbon dots in purified water, and fluorescence was collected for excitation wavelengths ranging from 280nm to 340nm, since the absorption profile of the carbon dots was observed to belong in that range. For what concerns metal containing solutions, two different metals were used to test fluorescent quenching: Fe(III) and Cr(III). Solutions with different concentrations of each metal were prepared and analysed, ranging from 25ppm to 500ppm. The quantity of carbon dots and water in these solutions was chosen equal to the solution containing only carbon dots, in order to achieve a clean comparison in between the fluorescence spectra. Fluorescent quenching was analysed at an excitation wavelength of 300nm, since the related fluorescence peak was observed to be the most responsive across the emission spectrum of the carbon dots. A satisfying and detectable quenched response was registered even down to 25ppm which, by comparison between the fluorescence spectrum of the carbon dots -only solution and the spectrum of the metal containing ones, demonstrated that carbon dots can be used as fluorescent probes for metal sensing.

# 1 Introduction

## 1.1 Carbon Dots: What they are

Carbon quantum dots (CDs) are a class of 0-dimensional carbon nanomaterials which in the last years gained great interest from the research point of view. The interest arose thanks to their novel and interesting properties, namely excellent photoluminescent behaviour<sup>1</sup>, high solubility thanks to the functional groups present on the surface<sup>2</sup> and size in the nanometre range<sup>3</sup>, namely 10 nm in diameter.

The most addressed fields of research are biology with particular effort on nanomedicine<sup>4,5,6,7</sup>, catalysts<sup>8,9,10</sup>, fillers for composites production<sup>11</sup> and photoluminescent sensing<sup>12,13</sup>, the latter being the focus of this thesis work. A summary image is reported in Figure 1.

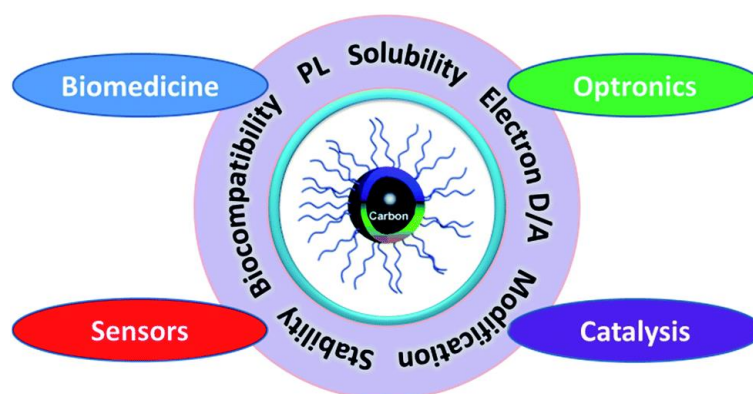


Figure 1: Fields of application for CDs (Reproduced with Creative Commons license).

In order address CDs, a first classification based on structural features can be made<sup>14</sup>:

- i) Graphene quantum dots (GQDs)
- ii) Carbon nitride quantum dots (CNQDs)
- iii) Carbon polymeric dots (CPDs)

GQDs present a core of  $\pi$ -conjugated parallel graphene planes surrounded by an oxidized shell<sup>15</sup>. On average the planes numbers are between 5 and 7. These types of CDs are conductive and present an almost spherical shape<sup>16</sup>.

CNQDs are similar to GQDs, meaning they are conductive and possess between 5 and 7 planes in the core, which however are more defected nitrogen-doped graphene planes<sup>17</sup>. Additionally, the external planes comprising the shell are not graphene-like.

Lastly, CPDs present no graphene-like layered structures but a polymeric carbon core<sup>18</sup>. They can be considered as not conductive if compared to GQDs<sup>19</sup> and contain heteroatoms in the core coming from the used precursors. They could possess oligomeric groups on the surface<sup>20</sup>. They can be divided in sub-categories depending on the synthesis parameters and precursors: this classification for CPDs is the most coherent among the existing ones.

A second classification is based on synthesis methods and will be further investigated in the following<sup>21</sup>.

A third and last classification is related to CDs properties such as emission wavelengths<sup>22</sup>, conjugation capabilities<sup>23,24,25</sup> and functionalities<sup>26,27</sup>, with the first being of particular interest from an applicative point of view. Still, this classification could make the other two cross over, generating ambiguity and thus is not the preferred one.

### 1.1.1 Hints on Discovery of Carbon Dots

As it is custom for major discoveries, CDs were first found by chance by Xu et al.<sup>28</sup> while working on single-walled carbon nanotubes (SWCNs).

Their work was focused on increasing the machinability of oxidized SWCNs without compromising their properties. The process was done by operating on their surface, mainly by electrophoretic techniques.

The purification resulted in a functionalization of the surface of SWCNs at the cost of a high degradation level that led to disruption of the nanotubes, ultimately leading to the formation of CDs. After spectroscopic analysis, an unexpected and strong fluorescence was observed coming from the samples, and its origin was attributed to the newly created CDs.

Since then, research on carbon dots has been greatly intensified.

### 1.1.2 Synthesis of Carbon Dots

Two different routes can be taken in the synthesis of CDs: top-down approach and bottom-up one, as reported in Figure 2.

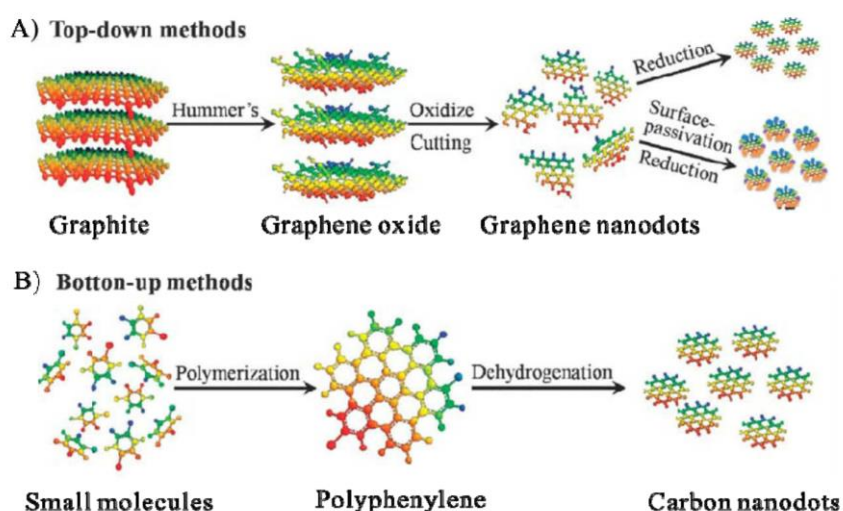


Figure 2: Top-down methods (A) and bottom-up methods (B) for the synthesis of CDs (Reproduced with permission)<sup>56</sup>.

The former operates on bulky carbon precursors that, through machining, lead to the formation of the nanoparticles. Some examples are LASER ablation, arc discharge and electrochemical techniques, in which CDs are obtained from carbon precursors such as graphite and carbon nanotubes.

The latter combines small organic molecules together such as carbohydrates or carbon nanocomposites in order to directly form the CDs. The most used bottom-up techniques are

microwave irradiation and hydrothermal carbonization, which vary in terms of temperature, energy and reaction time, giving rise to different types of CDs.

Both approaches require further purification steps in order to isolate the nanoparticles<sup>29,30</sup>.

The differentiation between these two routes can be used as a classification method for the CDs, but it is often overlooked since it does not account for CDs properties.

### 1.1.3 Properties of Carbon Dots

As stated above, CDs possess appealing properties that led to an intense research work around them since their discovery.

#### 1.1.3.1 Optical Properties

The most interesting and versatile property of CDs is the strong fluorescence emission<sup>31</sup>, together with a more general photoluminescent behaviour.

Before dealing with the photoluminescent behaviour of CDs, their light absorption properties will be discussed. The following Figure 3 depicts the absorption spectrum of the CDs together with the related electron transitions, belonging both to the core and shell electrons of the CDs<sup>32</sup>.

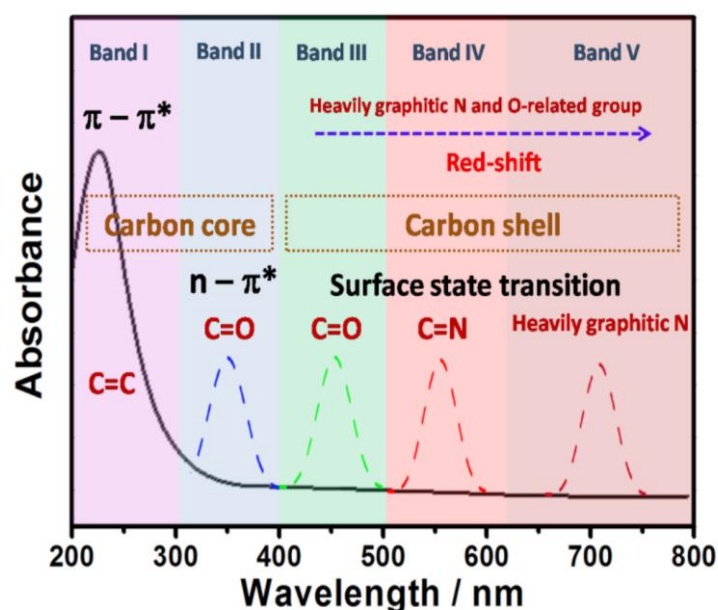


Figure 3: Absorption spectrum of CDs with related electron transitions (Reproduces with permission).

As it can be seen, the absorbance for wavelengths under 300 nm is related to the  $\pi$ - $\pi^*$  transitions, which involve aromatic  $sp^2$  carbons, meaning aromatic C=C bonds. In general, CDs possess strong UV absorption, with a tail extending into the visible range, occasionally even to the near-IR region.

For wavelengths between 300 nm and 400 nm the absorption is related to  $n$ - $\pi^*$  transitions, meaning intrinsic absorption of C=O bonds present in the cores.

For wavelengths greater than 400 nm, absorption is given by surface state transitions.

Moreover, the addition of graphitic nitrogen into the carbon core lattice red-shifts the absorption spectrum, due to nitrogen centres injecting electrons into unoccupied  $\pi^*$  orbitals, thus reducing the HOMO-LUMO gap<sup>33</sup>(HLG). Furthermore, absorption red-shifts also if functional groups containing oxygen are present on the shell of the CDs, such as carboxyl and hydroxyl ones<sup>34</sup>.

Let us focus now on the fluorescence properties of CDs.

The origin of fluorescence is still debated in the scientific community, but it is mainly attributed to quantum confinement. A schematic relating the dimension of the nanoparticle to its fluorescence behaviour is reported in Figure 4.

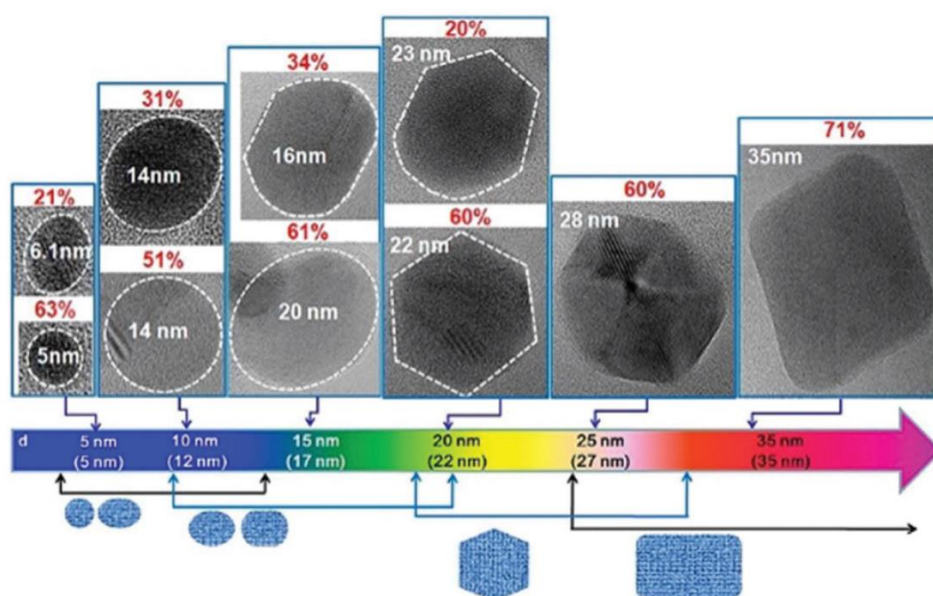


Figure 4: CDs fluoresce emission wavelength red-shift related to increasing CDs dimensions (Reproduced with permission)<sup>57</sup>.

Quantum confinement is a phenomenon related to the nanometric size of the particle, occurring when the Bohr radius of the exciton is bigger than the particle's average size<sup>35</sup>. This alters its energy profile, changing the conduction and valence bands from continuous to discrete. When conduction band electrons transition to an empty state (hole) in the valence band, they recombine emitting light, whose wavelength is dependent on the HLG value. Moreover, the smaller the particle, the bigger the HLG in between the bands, meaning a shift in the UV region and a higher quantum yield of emission<sup>36</sup>.

Conversely, for CDs with  $\pi$ -domains of greater size as in GQDs and CQNDs, fluorescence is mainly coming from conjugated  $\pi$ -electrons of condensed aromatic carbon domains. For larger  $\pi$ -domains the resulting HLG is smaller and thus the emission is red-shifted<sup>37</sup>.

Figure 5 depicts a general plot describing absorption and emission properties of CDs.

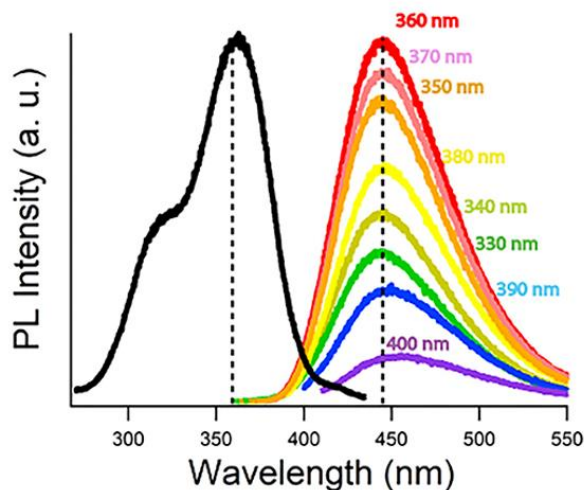


Figure 5: Absorption and emission spectra mock-up for CDs (Reproduced with Creative Commons license).

As investigated by Yu et al.<sup>38</sup>, other parameter acting on fluorescence are the core/shell size ratio of the CD and the presence of surface residues.

The surface defects generate surface states inside the HLG, effectively reducing it. They act as recombination centres for excitons, promoting radiative relaxation and thus generating multicolour emissions; for instance, blue emission is related to radiative recombination of excited electrons from the  $n-\pi^*$  transition, related to the C=O bonds. The emissions are red-shifted depending on the oxidation degree of the CD, meaning the content of oxygen-containing groups on  $sp^2$ -hybridized carbons<sup>39</sup>, as reported in Figure 6. This creates localized states below the  $\pi^*$  states, generating new energy levels in the gap: the reduction in HLG results in a higher emission wavelength. This emission mechanism is the primary one in CPDs since they don't present a proper graphitic core and do not rely on core-derived fluorescence. That being said, it is hypothesized that CPDs fluorescence could also derive from fluorophores residues from synthesis present on the dot or through the crosslink enhanced emission effect. In particular, emission fluorescence is magnified thanks to the formation of a rigid structure that negates intramolecular rotations, thus promoting radiative transitions and inhibiting vibrational (non radiative) ones<sup>40,41</sup>.

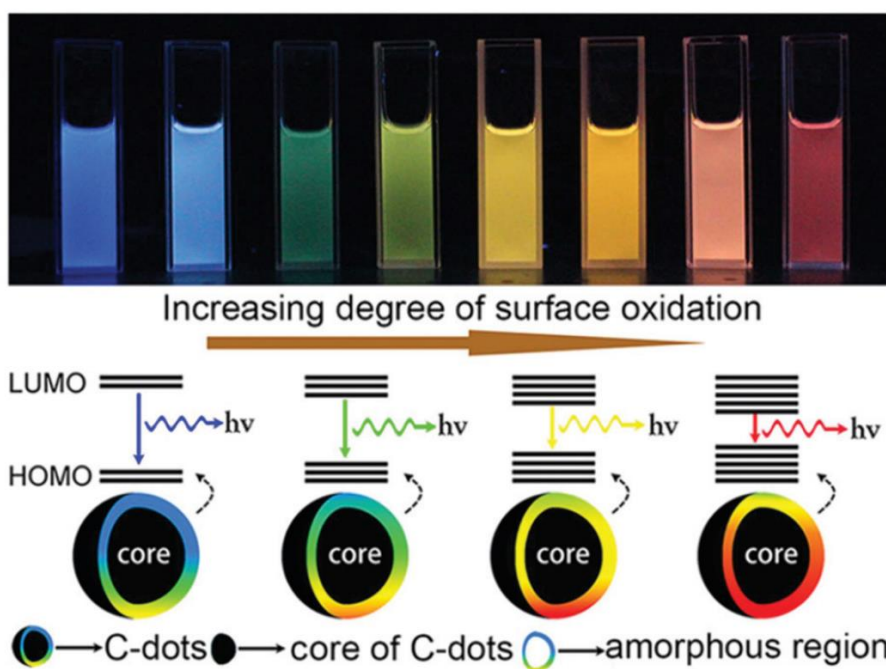


Figure 6: Fluorescent emission wavelength red-shift dependent on CDs increasing surface oxidation (Reproduced with permission)<sup>58</sup>.

Overall, CDs fluorescence can be exploited mainly by using the magnification effect or the quenching effect, with the latter being the focus of this thesis work, qualitatively depicted in Figure 7.

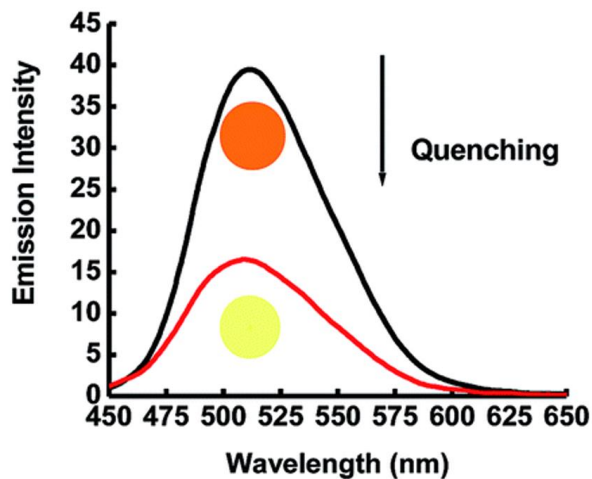


Figure 7: Fluorescence emission quenching phenomenon mock-up (Reproduced with Creative Commons license).

Fluorescence quenching is observed when the fluorescence emission intensity of a CD is reduced following a bond with another molecule, which will be the quencher molecule. The quenching effect is comprised of several quenching mechanisms:

- i) *Dynamic quenching (DQE)*<sup>42</sup>
- ii) *Static quenching (SQE)*<sup>43</sup>
- iii) *Photoinduced electron transfer (PET)*<sup>44</sup>
- iv) *Förster resonance energy transfer (FRET)*<sup>45</sup>
- v) *Dexter energy transfer (DET)*<sup>46</sup>
- vi) *Inner filter effect (IFE)*<sup>47</sup>
- vii) *Surface energy transfer (SET)*<sup>48</sup>

*Dynamic quenching* is given by the interaction between a diffusion quencher and the CD in its excited state, that results in a non-radiative energy transfer actuated by collision between molecules.

*Static quenching* involves the formation of a dark ground state complex between the CD and the quencher molecule.

*Photoinduced electron transfer* quenching takes place for distances greater than 10 nm between the CD and the quencher molecule, while *Förster resonance energy transfer* for distances lower than 10 nm and involves dipole-dipole coupling.

*Dexter energy transfer* is related to similar scale distances, but involves the overlap of the orbitals, meaning electron exchange between the CD and the quencher molecule.

*Inner filter effect* is also related to orbitals overlap between the excitation or emission spectrum of the CD and the absorption spectrum of the quencher.

Finally, *surface energy transfer* quenching is attributed to interactions between surface plasmons and the orbital system of a fluorophore. This type of quenching is more common for quantum dots than it is for CDs, but can happen also between CDs and small metal clusters.

CDs fluorescence quenching is a useful tool for the detection of metals or organic species: in this work, the former application will be treated.

Other than fluorescence, CDs could possess other photoluminescence mechanisms, namely phosphorescence and chemiluminescence. A scheme reporting radiative and non-radiative relaxation mechanisms is reported in Figure 8.

The former originates from the intersystem crossing going from the lowest excited singlet state level to triplet state and from radiative decay going from the lowest excited triplet state to the ground state one.

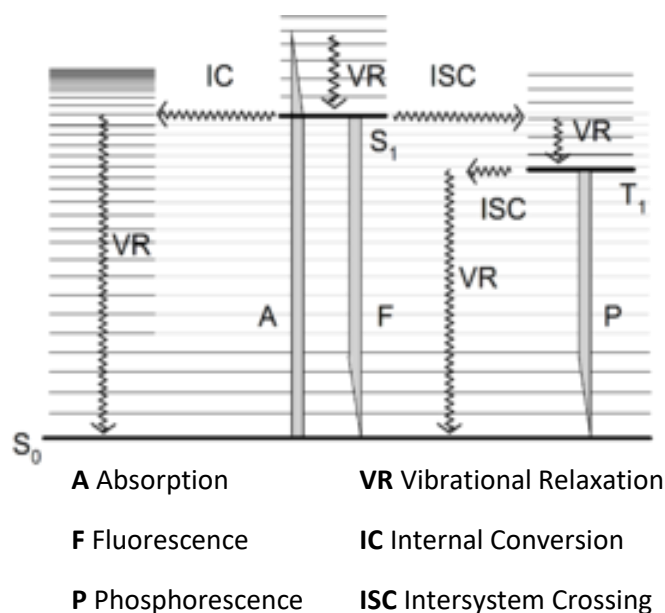


Figure 8: Possible radiative and non-radiative pathways (Reproduced with Creative Commons license).

The latter is produced during a chemical reaction, in which intermediate radical species decompose to form electronically excited species and then deactivate themselves; in CDs, chemiluminescence has its origin in fluorophore residues that behave as emitting centres, as reported by Lin et al.<sup>49</sup>.

As reported by Xu et al.<sup>50</sup>, the level of oxidation of the CDs influences their photoluminescent behaviour. In particular, high oxidized CDs showed high fluorescence emission with chemiluminescence, while poorly oxidized ones showed opposite behaviour. In conclusion, authors stated that fluorescence was related to the core states for photon absorption, with the shell behaving as a trap for long wavelengths, providing non-radiative recombination centres; conversely, chemiluminescence was related to radicals formed in the shell surface states.

### 1.1.3.2 Chemical Properties

The chemical properties of CDs vary with the structure of the CD itself.

Starting with GQDs, their chemical behaviour can be derived by using the Lerf-Klinowsky model for graphite oxide<sup>51</sup>. Their structure consists of layers of oxygenated graphene-like structure, in which strongly oxidized groups are concentrated on the edges, for instance carbonyls and carboxylic ones. GQDs can be functionalized by the addition of heteroatoms, which can be either integrated into the graphene-like structure during synthesis like nitride in CQNDs or added subsequently as doping agents. Moreover, they are soluble or at least dispersible in water media, generating colloidal suspensions.

GQDs structure is reported in Figure 9.

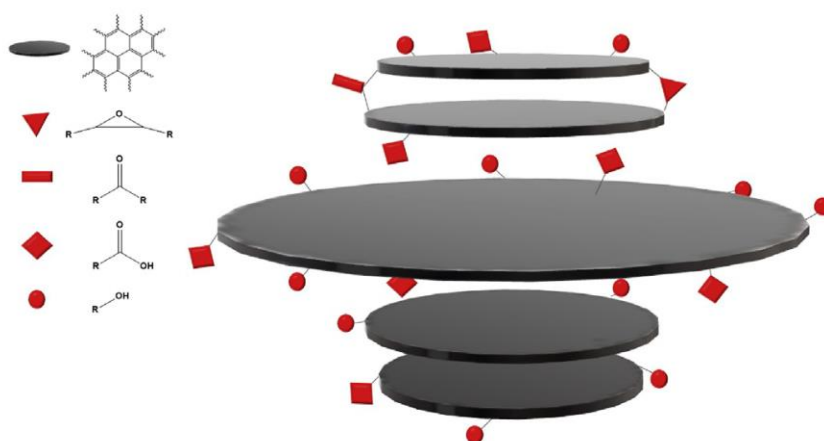


Figure 9: GQDs structure (Reproduced with permission).

CQNDs present the incorporation of nitrogen atoms into the graphene-like structure. However, their structure is complex: the use of strongly reactive precursors, such as urea, promotes formation of heptazine layers on the CD ends, which in turn change the structure of the CDs. Thanks to these functionalized edges, CQNDs are a very useful tool in the interaction with water media<sup>52</sup>. Their structure is described in Figure 10.

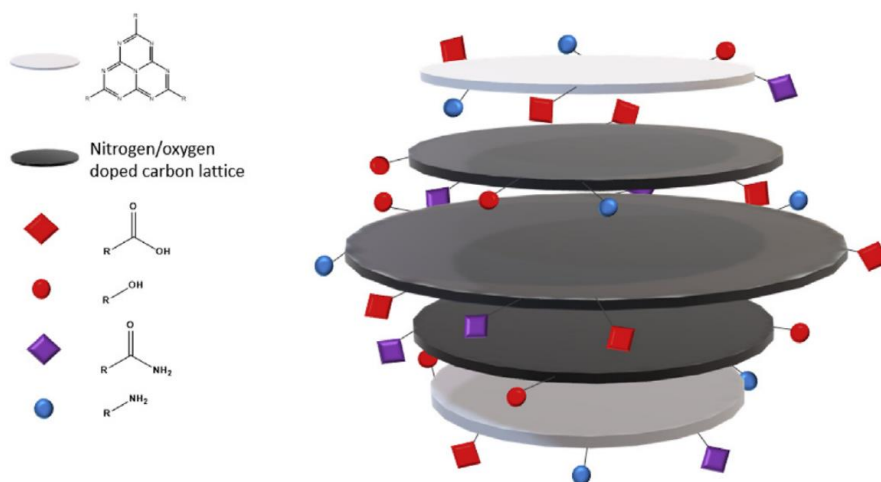


Figure 10: CQNDs structure (Reproduced with permission).

CPDs present more complex structures and can be divided into two main groups: CPDs produced by polymer degradation and CPDs produced by condensation of molecular units. The former partially retain the polymer original structure, but investigation on them is not yet on par with the other CDs, while the latter are easier to characterize. On this note, Mintz et al.<sup>53</sup> investigated and proved the presence of several mechanisms acting simultaneously during early chemical stages of CPDs synthesis. It followed that CPDs can't be treated as a well-defined and unique specie, rather a distribution of species which have chemical features shared among them. Figure 11 reports the structure for CPDs.

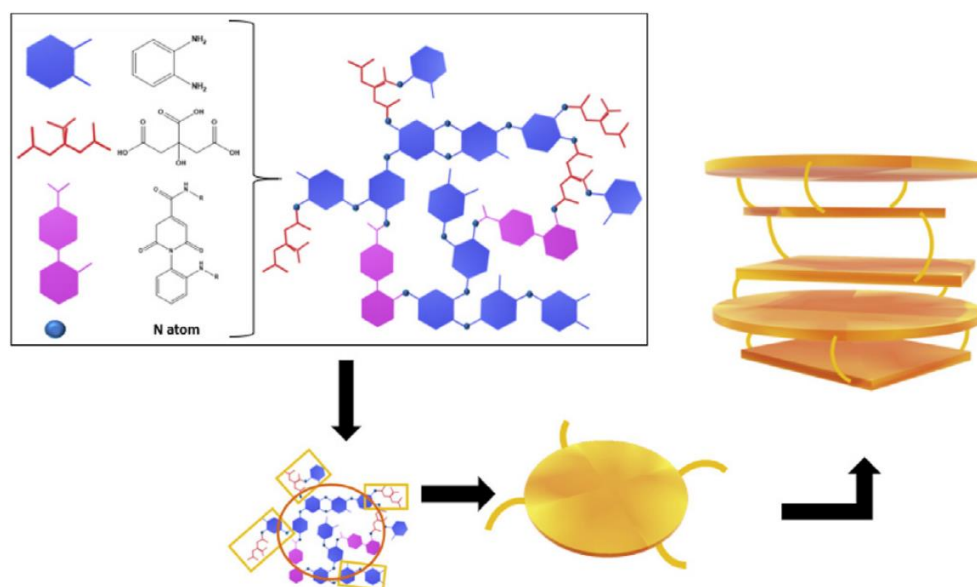


Figure 11: CPDs structure (Reproduced with permission).

In addition, as already mentioned, CPDs chemistry is also strongly dependent on synthesis conditions. For instance, Seven et al.<sup>54</sup> investigated the formation of glucose-based CPDs by using two different synthesis methods, namely microwave irradiation (MW) and hydrothermal carbonization (HT). Glucose took different pathways on the formation of the CDs, depending on the heating procedure given by the synthesis method.

In particular, MW promoted radical cleavage of acetal C-O bonds forming an intermediate, following multistep dehydration. The resulting compound could produce single ring aromatics through condensation or further dehydration steps. The formed species, namely aromatics and highly unsaturated ones, could form a structure by bonding to glucose residues or intermediates through C-O-C bonds. The preferential mechanism of radical cleavage is due to the short reaction time and high energy given by the microwave method.

On the other hand, HT promoted simple dehydration steps that led to the formation of the CDs after further condensation steps through aldol processes. The resulting CDs possess less functionalized aromatic cores and a higher thermal stability. More importantly, the resulting CDs could be classified as carbon nanodots (CNDs) rather than CPDs, which conversely are given from MW process.

## 1.2 Metal Sensing

A novel and interesting application is the use of CDs as fluorescent probes for the sensing of harmful metals, exploiting the fluorescence quenching effect. The use of CDs fluorophores is preferred with respect to inorganic semiconductor quantum dots and fluorescent dyes, because of their low toxicity and good biocompatibility<sup>55</sup>. Moreover, they are easier to produce also through green synthesis methods.

Metal sensing can be divided into solid phase sensing and solution phase sensing, where the former usually is applied to fingerprint sensing, film sensing, etc, while the latter can be adopted to sense anions and cations, small molecules and bio-molecules. In this thesis work, solution phase sensing will be employed to sense the presence of transition metal ions.

Transition metals possess, apart from a s-type orbital, incomplete d-type orbitals. They behave like electron-poor species and accept electrons from other chemical species, the electron-rich ones. In accepting the electrons, metals form metal-organic complexes with a series of organic molecules (O, N, S, ...) that possess a lonely electron pair, and the resulting bond will be species-dependant in terms of stability. This type of complexation is mediated by the  $\pi$ -d backbonding, in which the  $\pi$ -orbital of the organic molecule overlaps with the d-type orbital of the metal, allowing delocalization of electrons between the organic specie and the metal one.

Thus, by using CDs having specific chemical species on the shell, namely oxygen and nitrogen, the type of metal-organic complexes that can be formed is limited. In particular, only complexes with OH, carboxylic and amino groups are generated.

Following the formation of the metal-organic complex, fluorescence quenching can be observed and thus the presence of the metal can be sensed.

The type of quenching acting in this application is still debated. Given that it is related to the formation of a non-fluorescent metal-organic complex between the quencher and the fluorophore, the choice of the quenching mechanisms resides in static (SQE) and dynamic quenching (DQE), depending on the

fluorophore being in its ground state or excited state, respectively. A further, more thorough chemical analysis is necessary to assert the nature of the mechanism.

## 2 Aim of the work

The focus of the thesis work was to synthesize glucose-based carbon dots in order to employ them as fluorescent probes for harmful metal sensing. The chosen sensed metals were Fe(III) and Cr(III).

The sensing was made through the fluorescence quenching phenomenon, in which the intensity of the fluorescence emission of the CDs is reduced following a conjugation with a metal particle and the consequent formation of a metal-organic complex, and different concentrations for each metal were tested.

## 3 Materials and methods

In the following the used materials, adopted methods and characterization instruments will be addressed.

### 3.1 Materials: Reagents and instrumentation

The reagent used for the synthesis of the CDs is glucose, while the metals used for sensing come from iron nitrate  $\text{Fe}(\text{NO}_3)_3$  and chromium nitrate  $\text{Cr}(\text{NO}_3)_3$ .

The synthesis process required an autoclave and a hot plate for the carbonization process, while a dialysis membrane of 5 kDa cut-off and a magnetic plate for the purification step. Lastly, an oven was used to dry the sample solution, and a mortar to grind it.

### 3.2 Methods

#### 3.2.1 Synthesis of CDs

In order to obtain the CDs, a synthesis through hydrothermal method of glucose was adopted.

2 mg of glucose were mixed with 20 mL of distilled water. The solution was then put in an autoclave and heated up to 200°C on a hot plate for 5 hours. The autoclave was coated in aluminium foil in order to obtain a thermal coat to maintain and homogenize the distribution of heat.

Following the synthesis, the CDs were purified through dialysis with the use of a membrane with cut-off value of 5 kDa, meaning molecules smaller than 5 kDa could permeate. Dialysis was performed on a magnetic stirrer to favour the process, and the water was changed every 24 hours for a total of 72 hours of dialysis.

After dialysis, the solution was thermally treated in an oven at 60°C for several days, until the water fully dried off.

The last step was to lightly grind the CDs in a mortar in order to obtain a finer sample.

#### 3.2.2 Metal Conjugations

The chosen metals to be sensed, as abovementioned, are Fe(III) and Cr(III), coming respectively from  $\text{Fe}(\text{NO}_3)_3$  and  $\text{Cr}(\text{NO}_3)_3$ . In order to test the efficacy of quenching, seven solutions were prepared for

each metal, with different concentrations: 25 ppm, 50ppm, 100ppm, 200ppm, 300ppm, 400ppm, 500ppm. The solutions were prepared by mixing the specific quantity of metal (dependent on the ppm desired) with 100 mL of DI-H<sub>2</sub>O. Figure 12 depicts the prepared solutions.



Figure 12: Solutions containing Fe(III) (up) and Cr(III) (down).

Conjugation with CDs was made simply by dissolving 7 mg of CDs into 10 mL of metal solution, and manually stirring to favour the conjugation but not force it. The 0.7 mg/mL concentration was chosen since a clear fluorescence emission spectrum was analysed for the same concentration of a solution containing only the CDs.

### 3.2.3 Spectroscopic characterizations

For the characterization of the CDs several instruments were employed. First off, FTIR spectrometer to assess the quality of the material, followed by Raman spectroscopy to determine the chemical identity. UV-Vis analysis was performed to determine the absorption profile of the sample, while the fluorimeter was used both for the fluorescence analysis on the solution containing only CDs and for the study of the metal sensing through fluorescence emission quenching.

#### 3.2.3.1 FTIR analysis

IR spectroscopy was performed using a Thermo Nicolet 5700 FT-IR.

A background sampling of the air present in the laboratory was first performed, in order to subtract the related contributions from the spectrum of the CDs. Sampling of the FTIR spectrum for the CDs was then carried out with a cycle of 64 acquisitions, ranging from 500 cm<sup>-1</sup> to 4000 cm<sup>-1</sup>.

### 3.2.3.2 UV-Vis analysis

UV-Vis absorbance was measured with a PerkinElmer Lambda 35 UV/VIS Spectrometer.

The analysis was performed for wavelengths ranging from 380 nm to 800 nm, meaning from visible light to near-IR.

The mass extinction coefficient  $\varepsilon_\lambda$  has been calculated through the Lambert-Beer law,

$$A = \varepsilon_\lambda l \rho$$

where  $A$  is the absorbance,  $l$  is the optical path and  $\rho$  is the mass concentration.

By plotting the absorbance  $A$  against the solution concentration, the coefficient was found by imposing an interpolating line forced at the axis origin: the slope of the line corresponded to the mass extinction coefficient times the optical path length,  $\varepsilon_\lambda \cdot l$ .

Following the mass extinction coefficient, the absorption coefficient  $\alpha$  has been calculated through the formula:

$$\alpha = \frac{4 \pi \varepsilon_\lambda}{\lambda}$$

Where  $\lambda$  are the wavelengths corresponding to the peak intensity for each emission curve.

Lastly, the natural logarithm of  $\alpha$  has been plotted against the excitation energies and fitted with a parabolic interpolation, finally yielding the width  $\sigma$  of the  $\Pi$  band as the second order coefficient of the interpolated curve.

The width  $\sigma$  can also be correlated with the order of the system<sup>53</sup>.

### 3.2.3.3 Fluorescence analysis

The fluorescence emission response of the CDs was collected with a PerkinElmer LS55 Fluorescence Spectrometer, using a fluorescein-based method. The entrance and exit slits were imposed to be 5 nm and the scan speed 50 nm/s, in order to obtain more precise measurements.

A solution of 0.7 mg/mL for CDs in DI-H<sub>2</sub>O was prepared. The spectrum of this solution containing only CDs was collected for wavelengths going from 300 nm (4.13 eV) to 600 nm (2.07 eV), since the emission band was observed to be in that range. For the excitation wavelengths, the values were chosen from 280 nm (4.42 eV) to 340 nm (3.64 eV) with a step of 10 nm. High-pass filters were imposed accordingly to the excitation wavelength used in order not to have artifacts in the emission spectrum.

For what concerns the solutions containing the metal-conjugated CDs, the quenched response was measured at an excitation wavelength of 300 nm because it was found to be the most responsive to the quenching effect. The remaining instrument parameters were maintained unchanged.

#### 3.2.3.4 Raman analysis

Raman spectroscopy was performed using a Renishaw Invia Spectrometer.

Two acquisitions were performed employing a red LASER with wavelength equal to 785 nm. The exposition time was 10 seconds and the applied power was equal to 2.5 mW.

## 4 Results

### 4.1 Synthesis Process

As reported by Seven et al.<sup>54</sup>, glucose-based CDs synthesised by hydrothermal method may be classified as carbon nanodots (CNDs). CNDs are a broader subtype of CDs, defined as small carbonized quasi-spherical nanoparticles which do not possess a proper crystal core, but an ordered one resembling the graphitic, and are functionalized on the shell.

In the following a description of the process pathway will be given.

A schematic of the glucose molecule is provided in the following Figure 13.

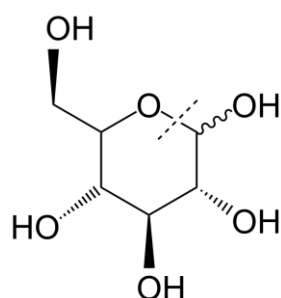


Figure 13: Glucose molecule chemical structure.

By heating up the solution through hydrothermal method, the glucose molecule undergoes a dehydration process producing the following reaction intermediates, reported in Figure 14.

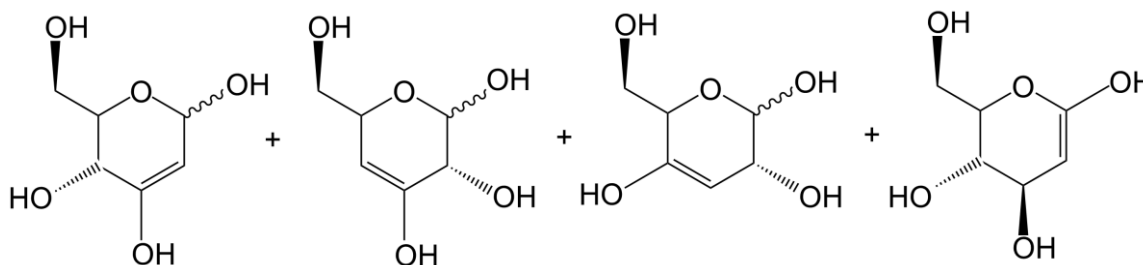


Figure 14: Species after dehydration process.

The process leads to the formation of the following species, reported in Figure 15.

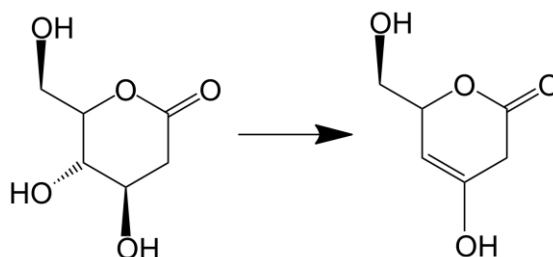


Figure 15: Species formed with the ongoing of the reaction.

These species then condense through aldol process forming the specie reported in Figure 16, that could lead to the formation of less functionalized aromatic cores.

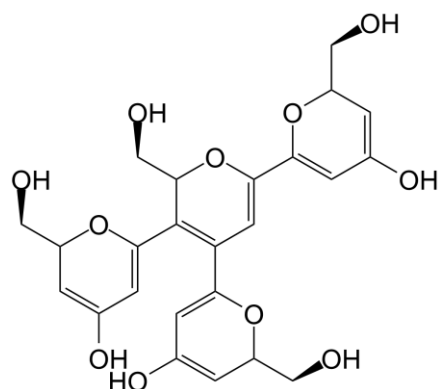


Figure 16: Species after aldol condensation.

Further dehydration and aldol reactions occur on the external edges of the structure, leading to its enlargements.

Finally, these species undergo further condensation and dehydration processes, leading to the formation of aromatic rich domains.

The resulting core and shell structures of the synthesised CDs are both reported in Figure 17.

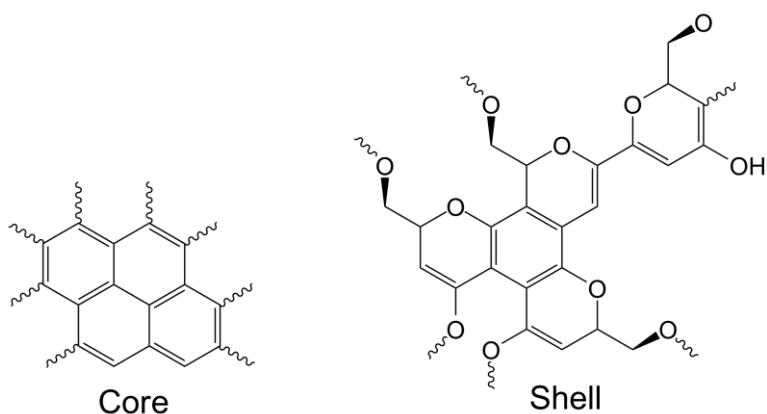


Figure 17: Chemical structure for CDs core (left) and shell (right).

A schematic of the complete process pathway is reported in Figure 18.

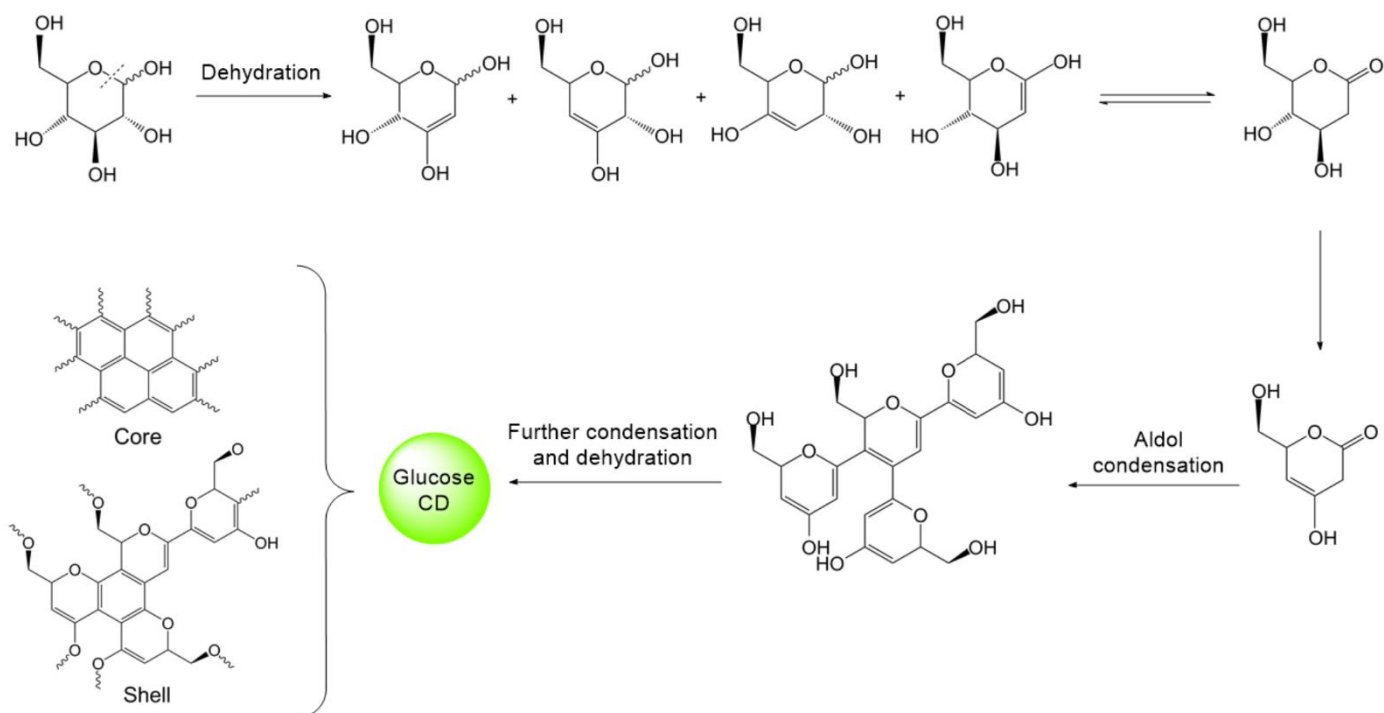


Figure 18: Process pathway of CDs synthesis through HT method.

## 4.2 Spectroscopic Characterizations

### 4.2.1 FTIR Analysis

The first analysis performed on the synthesised dots was the infrared spectrometry<sup>59</sup>. The resulting spectrum is reported in Figure 19.

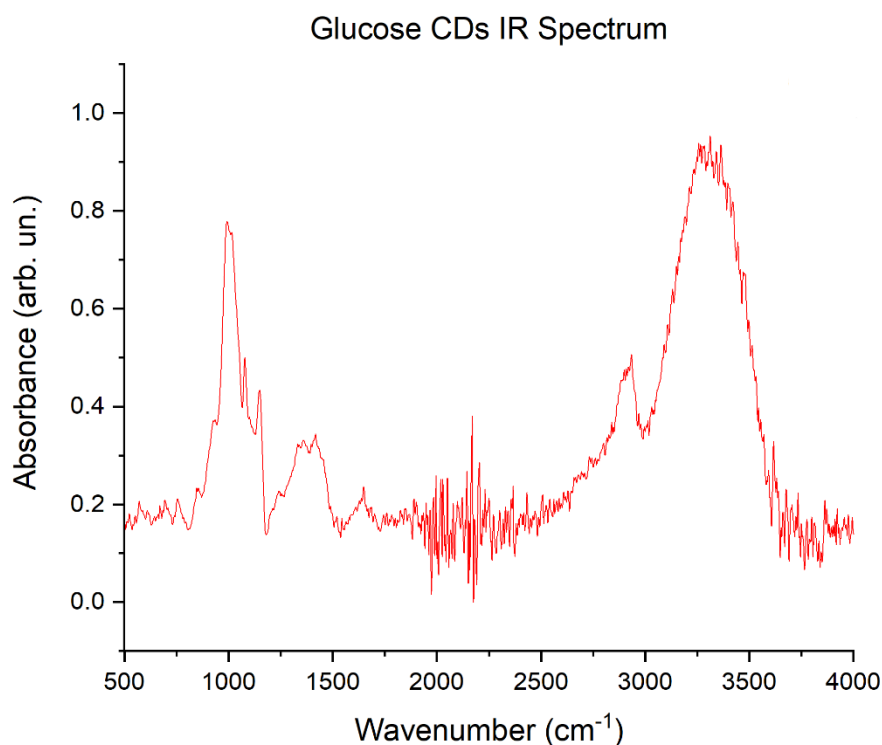


Figure 19: IR spectrum of glucose CDs.

Starting from 750 cm<sup>-1</sup>, the bands seen up to 1500 cm<sup>-1</sup> are related to  $\nu_{C-C}$  and  $\nu_{C-O}$  of single bonds between carbons and between carbon and oxygen.

The band at around 1660 cm<sup>-1</sup> is related to  $\nu_{C=C}$  of double bonds between carbons, thus from the aromatic domains, while the ones between 1700 cm<sup>-1</sup> and 2000 cm<sup>-1</sup> derive from  $\nu_{C=O}$  of double bonds between carbon and oxygen. This on the other hand indicates that functional groups are formed on the shell of the nanoparticles, namely carboxylic, carbonyl and ester ones.

The noise in between 2000 cm<sup>-1</sup> and 2500 cm<sup>-1</sup> is expected and is related to carbon dioxide present in the laboratory environment, while the last two bands can be seen for 2750-3000 cm<sup>-1</sup> and 3000-3500 cm<sup>-1</sup> ranges. Both are related again to single bonds, with the former being  $\nu_{C-H}$  between carbon and hydrogen while the latter  $\nu_{O-H}$  between oxygen and hydrogen.

From the analysis it can be concluded that the CDs present aromatic domains in the core and functional carboxylic groups on the outer shell. The spectrum is in accordance with the literature.

#### 4.2.2 UV-Vis analysis

For the UV-Vis analysis<sup>60</sup>, the solution was prepared with 0.6 mg of CDs in 16 mL of DI-H<sub>2</sub>O.

The normalized UV-Vis absorption spectrum has been plotted in the following Figure 20.

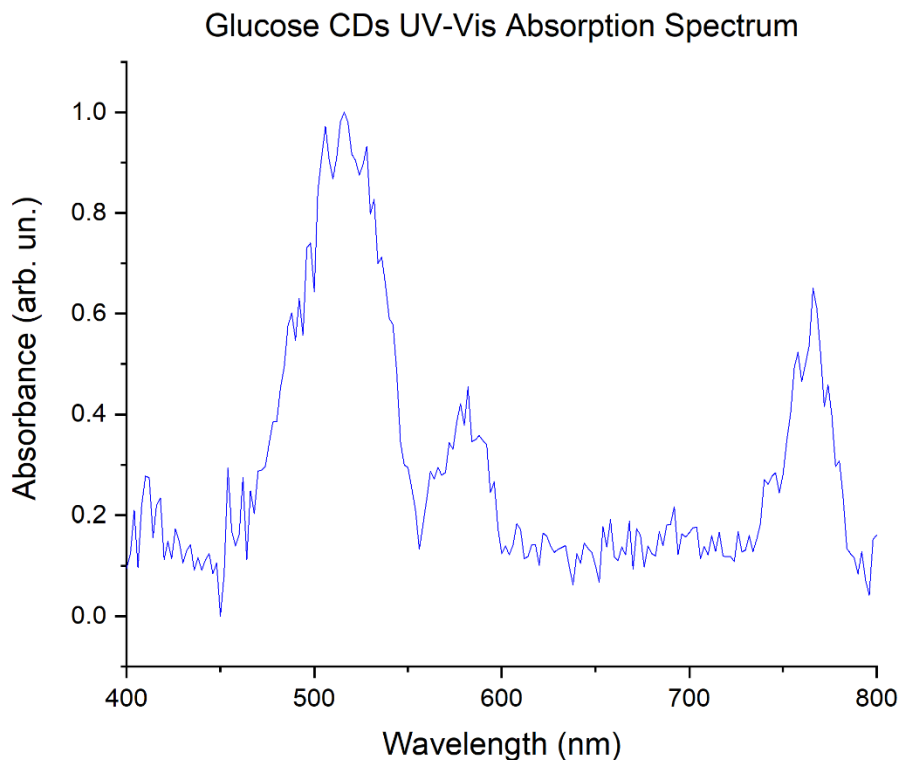


Figure 20: UV-Vis absorption spectrum of glucose CDs.

The small absorption peaks at 400 are attributed to the  $n-\pi^*$  transitions of C=O bonds.

The absorption band at 520 nm derives from the semi graphitic core of the nanoparticle, confirming that glucose CDs made by HT method are resembling the more ordered structure of the CNDs.

Lastly, the bands at around 580 nm and 780 nm come from the presence of aromatic systems of different dimensions.

Through Lambert-Beer law, the mass extinction coefficient  $\epsilon_\lambda$  has been calculated.

Absorbance  $A$  was taken as the peak value of the spectrum, the optical path  $l$  corresponded to the lateral dimension of the cuvette holding the solution, meaning 1 cm, and concentration  $\rho$  was calculated as mass of the CDs over the solvent volume.

The resulting mass extinction coefficient is  $\epsilon_\lambda = 3.68 \cdot 10^5 \text{ m}^2 \text{ g}^{-1}$ , which is in line with the existing literature.

Lastly, the width  $\sigma$  of the  $\Pi$  band has been calculated as per described in the “Methods” paragraph, resulting in  $\sigma = 0.039 \text{ eV}$ . The dimension of  $\sigma$  is strictly correlated to the degree of disorder of the system, meaning that a smaller  $\sigma$  yields a lower degree of disorder, thus a higher order of the system.

The calculated  $\sigma$  can be regarded as relatively small, thus acting as a further confirmation that the synthesised CDs possess a somewhat ordered core akin to a graphitic one.

#### 4.2.3 Fluorescence analysis

The most important characterization for this thesis work was the fluorescent response of the CDs<sup>61</sup>.

The emission spectrum is the following, Figure 21.

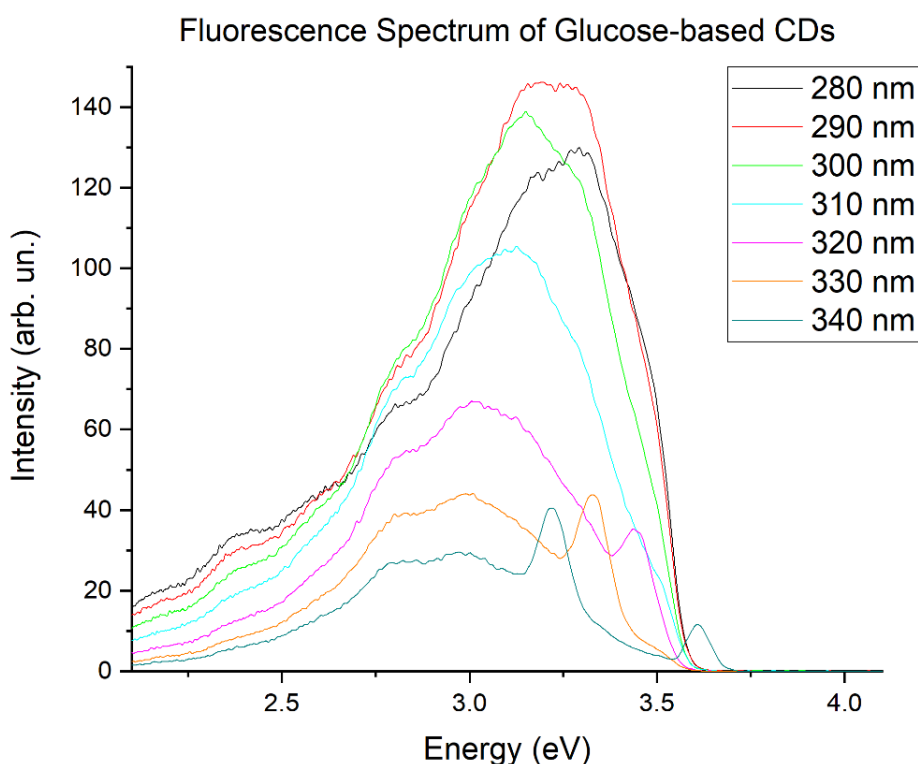


Figure 21: Fluorescence emission spectrum (in eV) of glucose CDs.

Overall, emission is localized between 2.75 eV up to 3.55 eV, meaning in the range comprising blue visible light and the low-end of the ultraviolet.

It can be noticed that two peaks are present in the band, one at smaller energies with a lower intensity (1) and the other at higher energies, with peak intensity (2).

This is due to the superposition of two bands in the emission spectrum, one excitation-independent, from which the peaks labelled with “1” come from, and one excitation-dependent, from which conversely originate the peaks labelled with “2”. The labelled spectrum is reported in Figure 22.

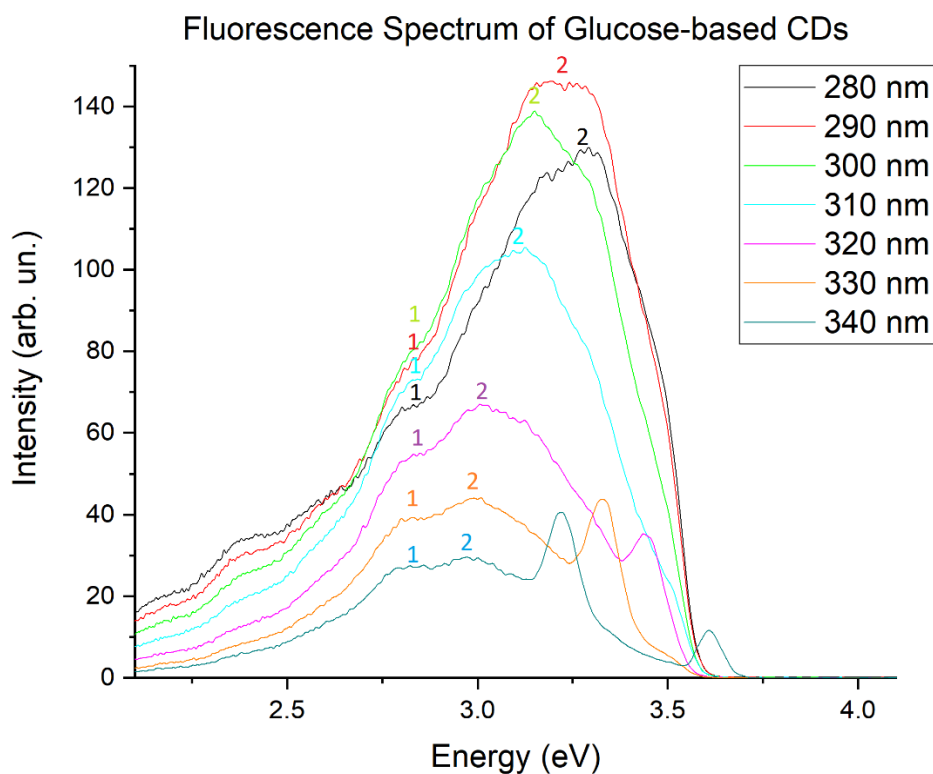


Figure 22: Fluorescence emission spectrum (in eV) of glucose CDs with labelled peaks.

The excitation independent peaks are centred around 2.8 eV, while the dependent ones range from 3.0 eV to 3.4 eV, approximately. The former, given the lower energies, could be attributed to  $n-\pi^*$  transitions inside the band, due to energy states formed inside the HLG given by the functional groups on the shell of the CDs; the latter, conversely, possess higher energies and are associated to  $\pi-\pi^*$  transitions occurring in the graphitic-like core of the CDs.

In order to better appreciate the dependency or lack thereof with respect to the excitation energy, two plots have been made, both relating the excitation energy to the emission energy sampled at peak intensity.

For what concerns the “1” peaks, the following plot is found, Figure 23.

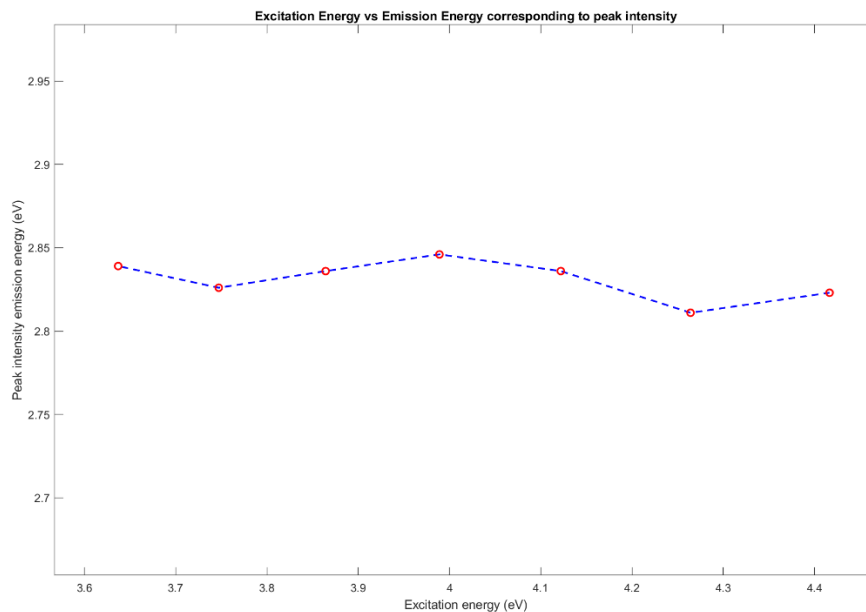


Figure 23:  $E_{ex}$  vs  $E_{em\_peak}$  for "1" label peaks.

It can be seen that the overall behaviour of the curve is a piecewise line parallel to the x-axis, meaning the excitation energy. This indicates that the related band is excitation-independent, since the emission energy is maintained equal independently from the excitation energy.

Conversely, relating to peaks labelled with "2", Figure 24.

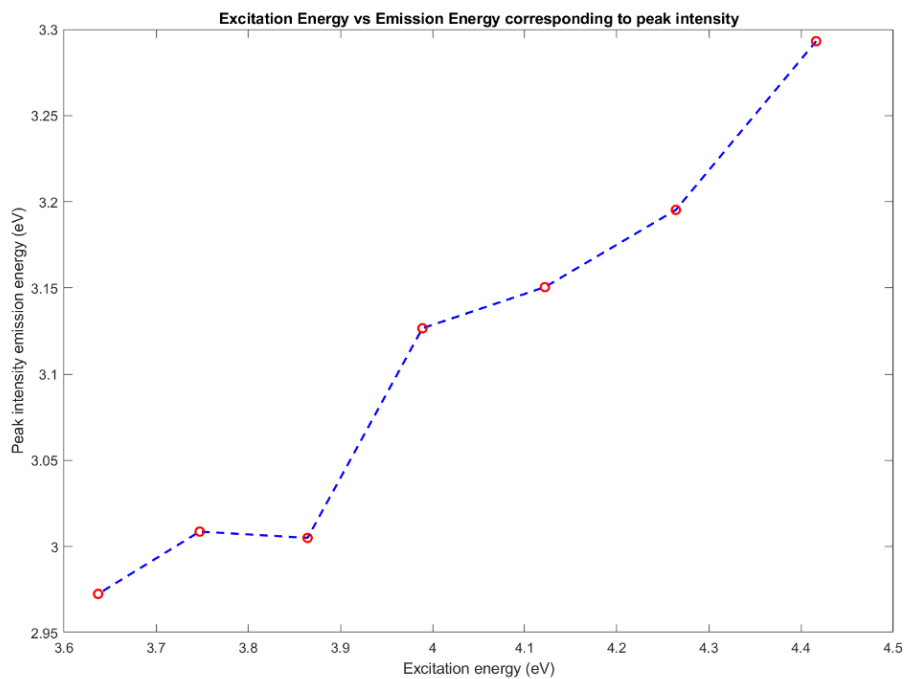


Figure 24:  $E_{ex}$  vs  $E_{em\_peak}$  for "2" label peaks

The obtained curve increases with increasing excitation energy, meaning the emission energies mostly increase with the energy of the excitation LASER. It can thus be stated that the related energy band is excitation-dependent. This band will be the chosen one for the quenching applications, since it showed better response to metal conjugations and a wider range of fluorescence intensities.

It is to note that the small, sharp peaks between 3.25 eV and 3.75 eV, reported in Figure 25, are to be attributed to the high-pass filter not completely blocking the excitation wavelength and should not be taken into account for characterization considerations.

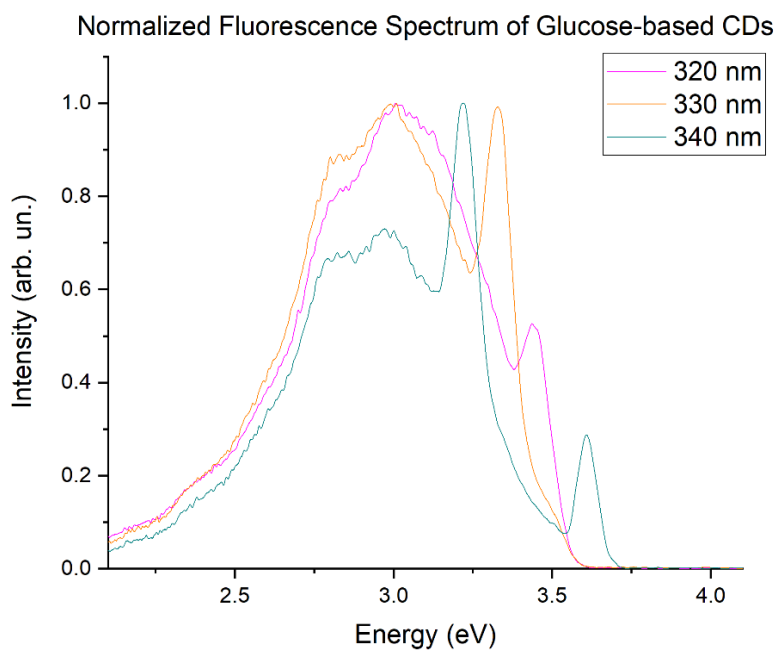
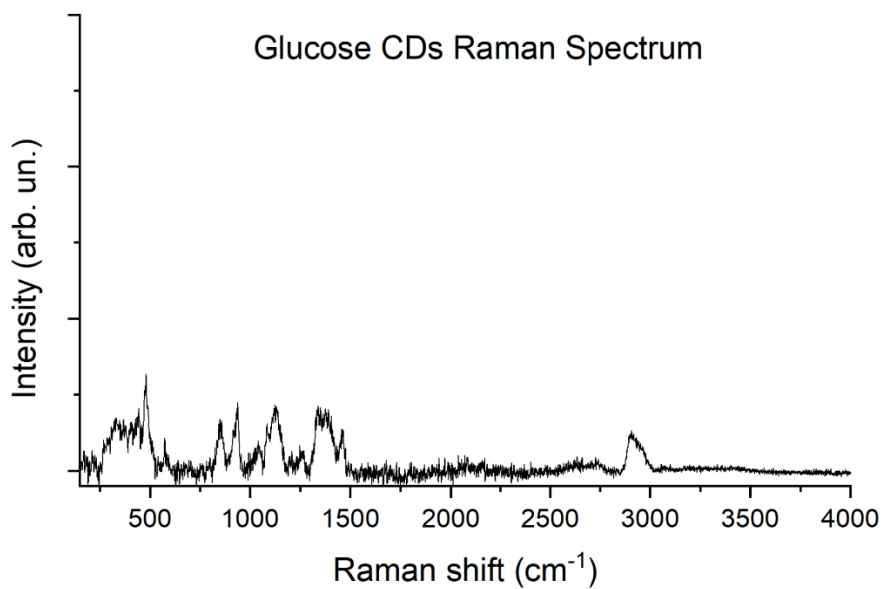


Figure 25: Zoom on normalized fluorescence spectrum (in eV) of glucose CDs depicting filter artifacts.

#### 4.2.4 Raman Analysis

Raman spectroscopy was performed on CDs samples to assess their chemical identities<sup>62</sup>.

The resulting spectrum is reported in Figure 26.



*Figure 26: Raman spectrum of glucose CDs.*

Different bands can be observed from the spectrum, which have been labelled in the following for easiness of discussion in Figure 27. Differently from the FTIR spectrum, Raman spectrum isn't as straightforward to discern, thus hypothesis will be made.

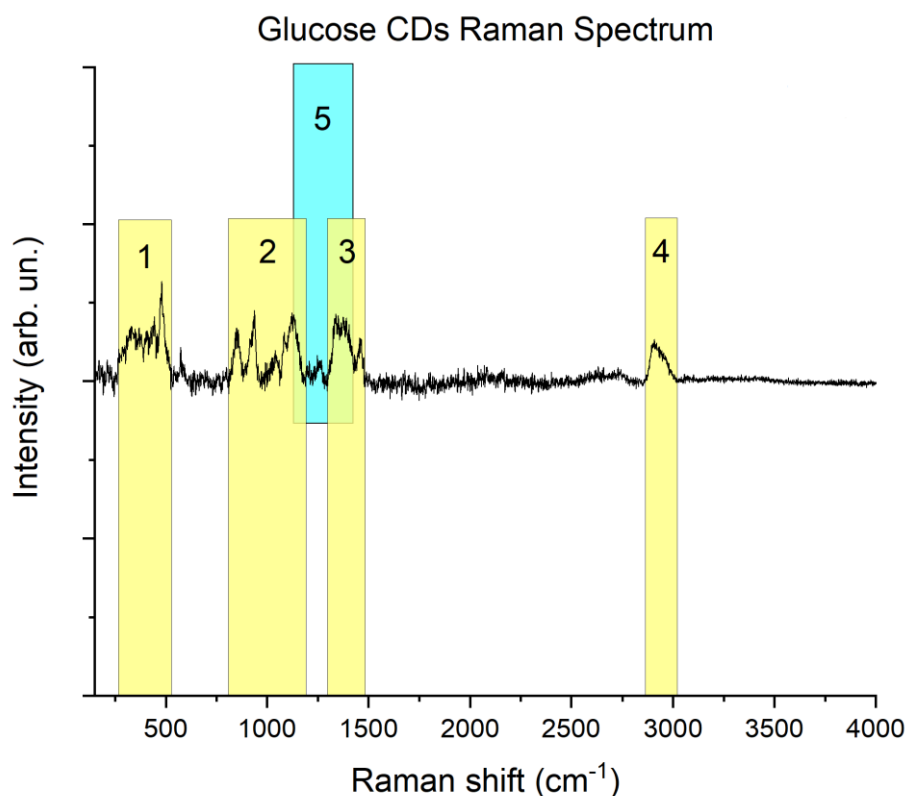


Figure 27: Raman spectrum of glucose CDs with labelled peaks.

The band between 250 cm<sup>-1</sup> and 500 cm<sup>-1</sup>, which has been labelled with “1”, contains peaks which are to be attributed to skeletal vibrations of the aromatic structures of the CDs, which can be hypothesised to reside in the core. Moreover, in the range between 750 cm<sup>-1</sup> and 1250 cm<sup>-1</sup>, label “2”, the peaks are associated with the Raman shift given by aromatic rings, again belonging to the core. From these considerations it could be concluded that the synthesised CDs possess in fact an aromatic core.

Band labelled “3”, meaning from 1250 cm<sup>-1</sup> up to 1500 cm<sup>-1</sup>, contains peaks related to the shift given by single C-C bonds. The peak related to the highest shift between 2800 cm<sup>-1</sup> and 3000 cm<sup>-1</sup>, label “4”, comes from aromatic CH functional groups. Lastly, peaks in the band labelled “5”, around 1200 cm<sup>-1</sup> and 1500 cm<sup>-1</sup>, are more difficult to treat due to superposition with other peaks, but they are assumed to come from functional groups such as CH<sub>2</sub> and CH<sub>3</sub>. In this case, the results could be attributed with the formation of a functionalized shell of the CDs.

Overall, given the proposed hypothesis, the Raman analysis is coherent with the expected structure of the CDs.

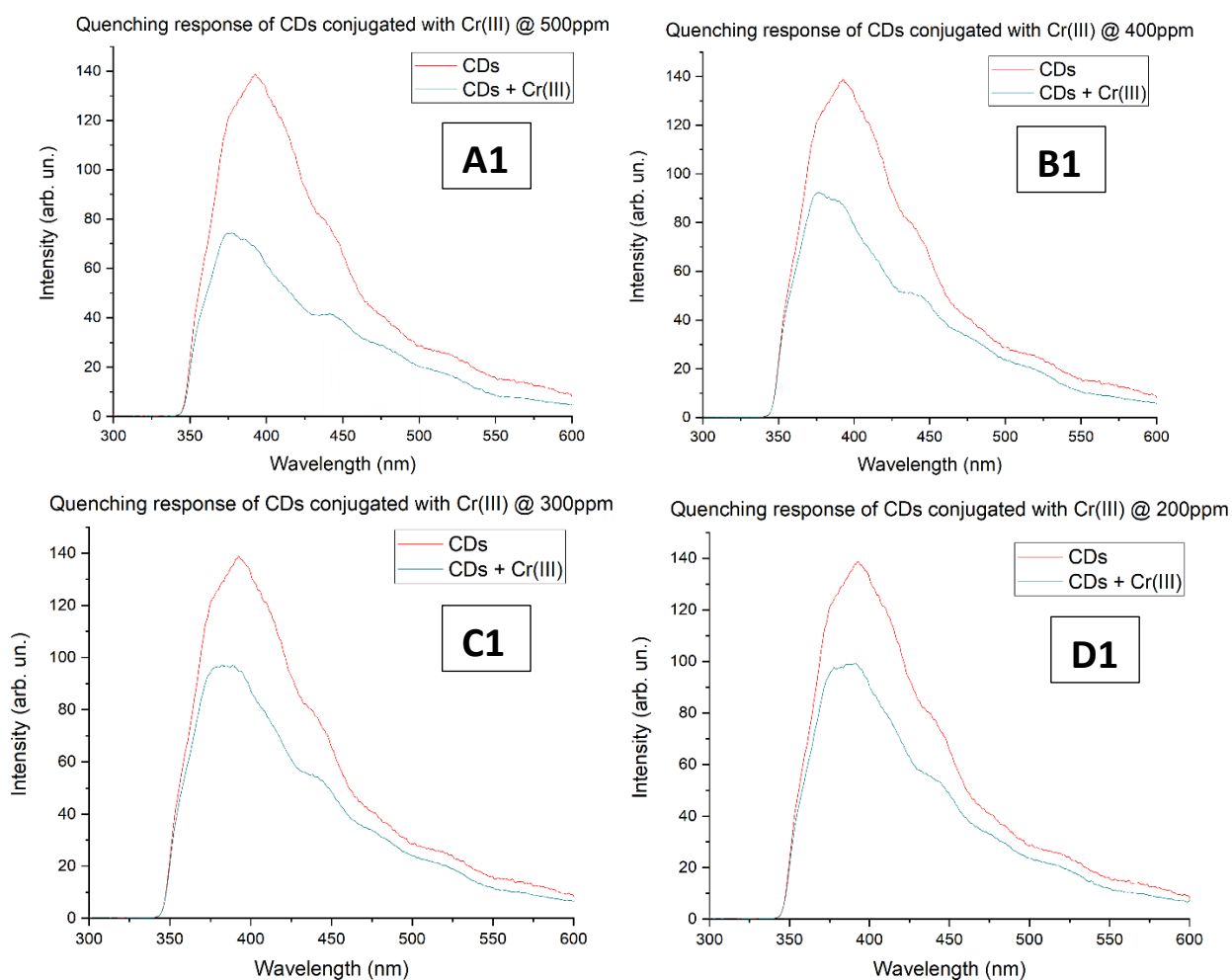
### 4.3 Metal Sensing

Metal sensing was done through a fluorescence analysis. Metal conjugation with the CDs was made for each solution concentration, and the fluorescence response was measured. Each measurement was performed three times in order to have more accuracy, and the final plot was taken as a mean of the three.

#### 4.3.1 Cr(III) Sensing

The first performed was the sensing of Cr(III).

In the following the quenched response is reported for each decreasing concentration of the metal in solution, along with the fluorescence at 300 nm for comparison, Figure 28 from (A1) to (G1).



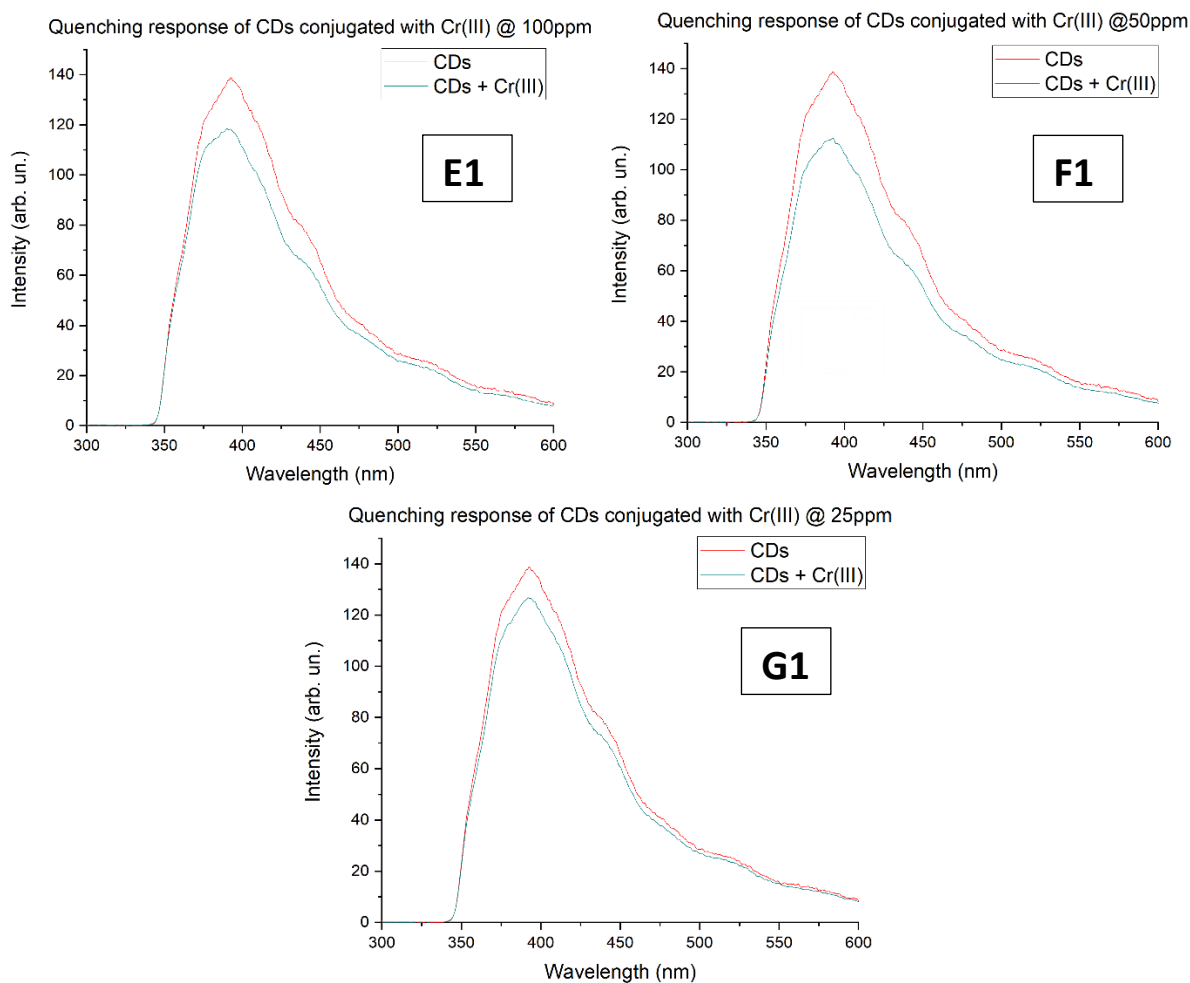


Figure 28: Quenching response of Cr(III)-conjugated CDs varying with metal concentration.

(A1) 500 ppm (B1) 400 ppm (C1) 300 ppm (D1) 200 ppm (E1) 100 ppm (F1) 50 ppm (G1) 25 ppm

From the plots an appreciable quenching effect can be seen. The quenching is more prominent for higher concentrations of the metal in solution, as expected, but a measurable difference can be also seen for the lower end of the concentrations, namely 25 ppm.

It is also to notice that, for the second to last lower concentration, the quenched response varies in time. This could be related to the lower effective number of metal molecules in the solutions. It may have made complexation with CDs more difficult, meaning that CDs required more time in order to bond with the metal particles and consequently increase the quenching effect.

The behaviour is made explicit in the following plot in Figure 29.

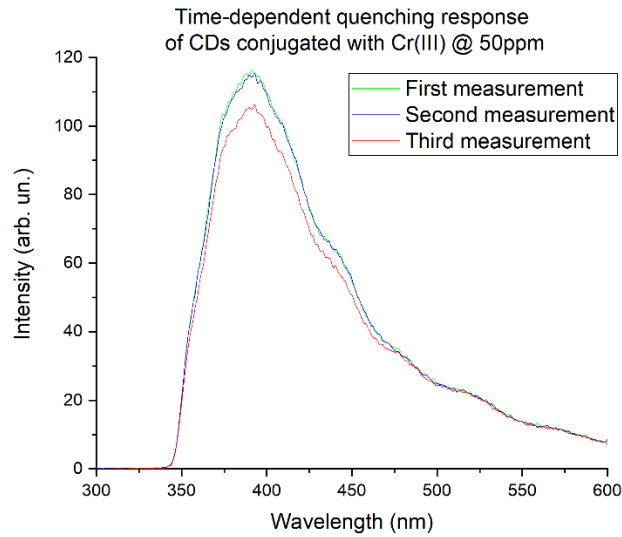
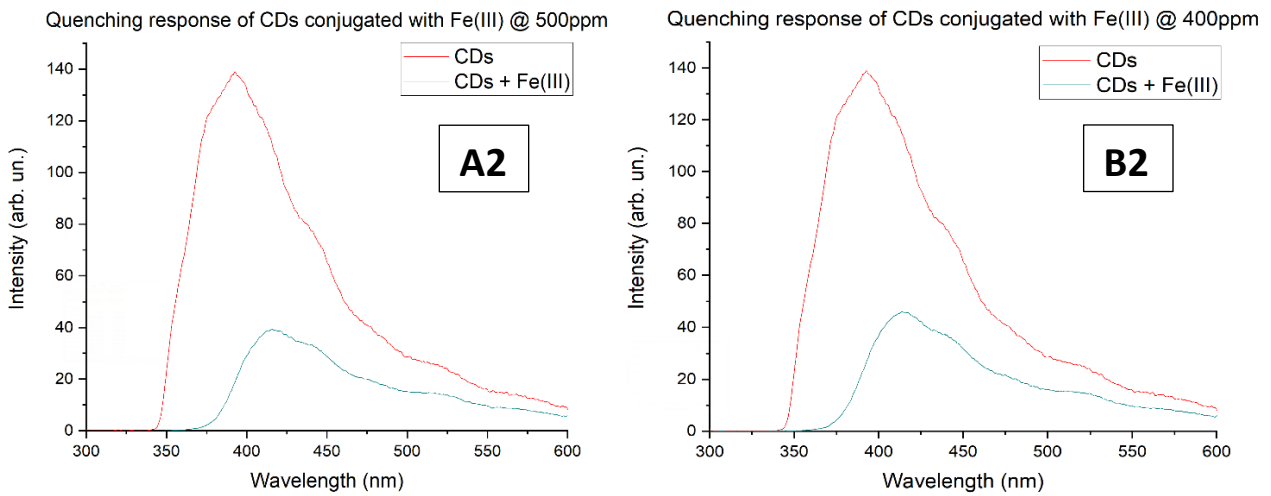


Figure 29: Time dependent quenching response of Cr(III)-conjugated CDs for 50 ppm metal solution.

#### 4.3.2 Fe(III) Sensing

The same steps were performed for Fe(III) solutions, and the quenched response was plotted with the CDs fluorescence at 300 nm, in Figure 30 from (A2) to (G2).



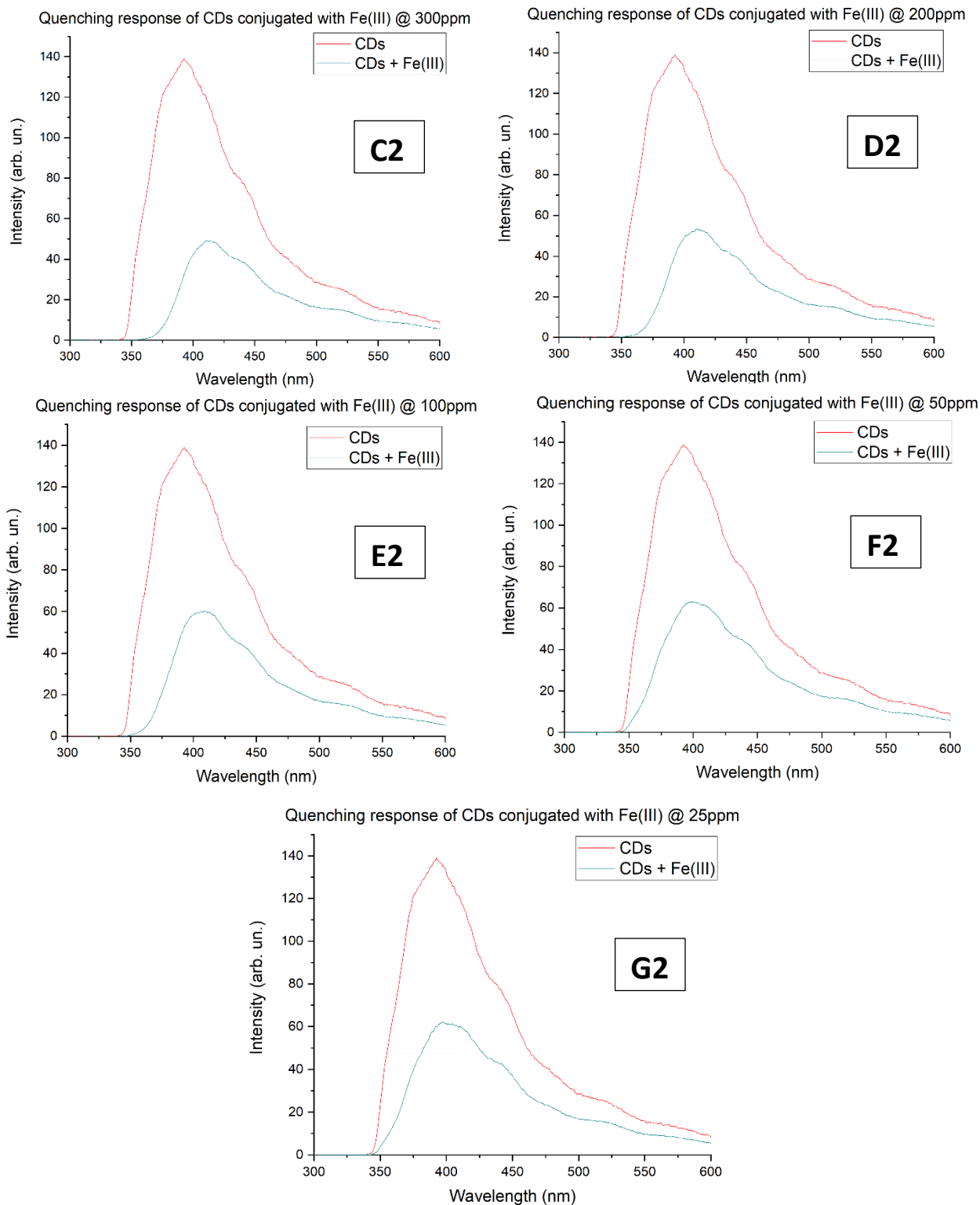


Figure 30: Quenching response of Fe(III)-conjugated CDs varying with metal concentration.

(A2) 500 ppm (B2) 400 ppm (C2) 300 ppm (D2) 200 ppm (E2) 100 ppm (F2) 50 ppm (G2) 25 ppm

Similarly to the case with Cr(III), the quenching is more present with higher metal concentrations. In the case of Fe(III), though, the effect of metal conjugation is far stronger, and a highly measurable quenching response can be observed and measured even at 25ppm.

Again, for 25ppm and 50ppm, the quenching response is time dependent, as can be seen in Figure 31.

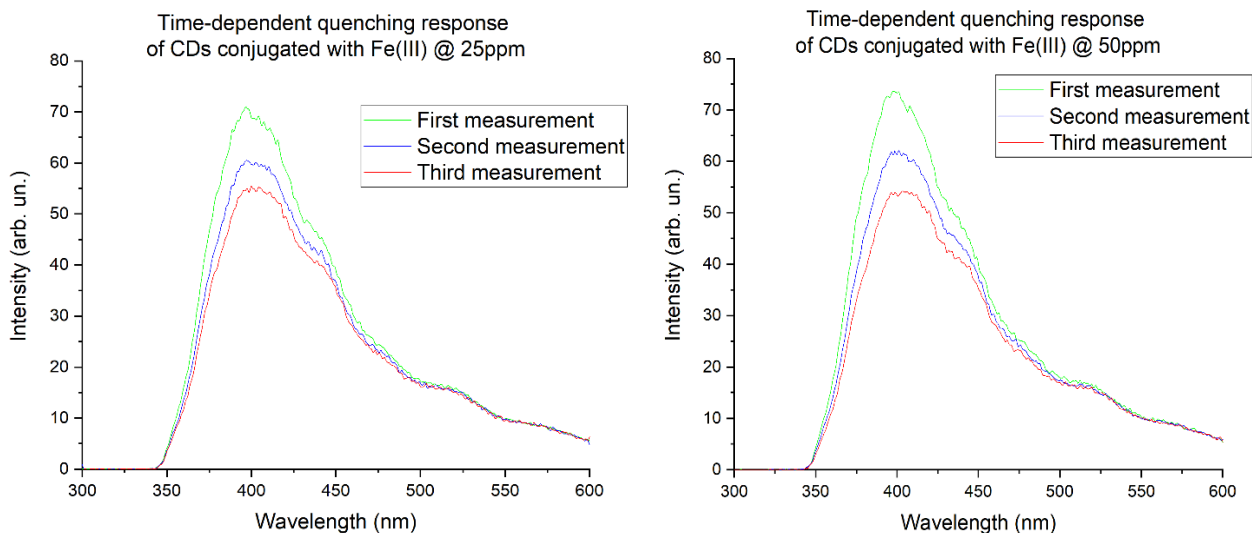


Figure 31: Time dependent quenching response of Fe(III)-conjugated CDs for 25 ppm (left) and 50 ppm (right) metal solution.

#### 4.3.3 Quenching Comparison

In order to compare the quenching behaviour of the two metals, calibration curves have been made.

The peak quenched intensity was registered for each metal concentration and subtracted to the peak fluorescence intensity at 300 nm of the solution containing only CDs, because it showed better quenching response. Lastly, the difference was divided by the peak intensity of the CDs and the values were plotted against the concentrations, yielding a calibration plot.

The calculated values are reported in the following Table 1.

Table 1: Peak intensity difference for each metal at different solutions concentrations.

	25 ppm	50 ppm	100 ppm	200 ppm	300 ppm	400 ppm	500 ppm
Cr(III)	0.08	0.19	0.15	0.28	0.30	0.33	0.46
Fe(III)	0.55	0.54	0.56	0.61	0.64	0.67	0.72

For this purpose, the highlighted values of intensity difference at 50 ppm for Cr(III) and at 25 ppm for Fe(III) haven't been considered, because the former was an outlier point and the latter was out of linearity range.

The following plot have been obtained with a linear interpolation, Figures 32 and 33.

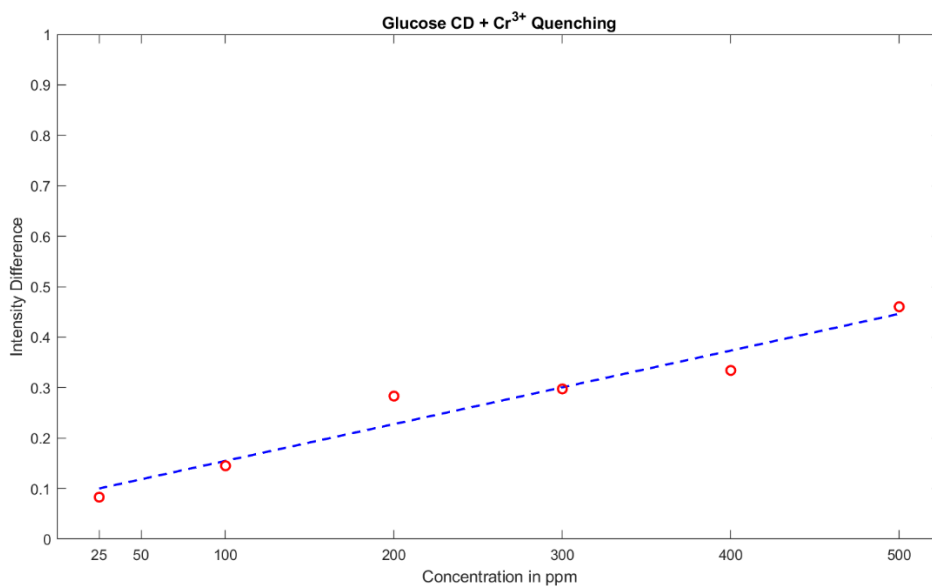


Figure 32: Calibration curve for Cr(III)-related quenching.

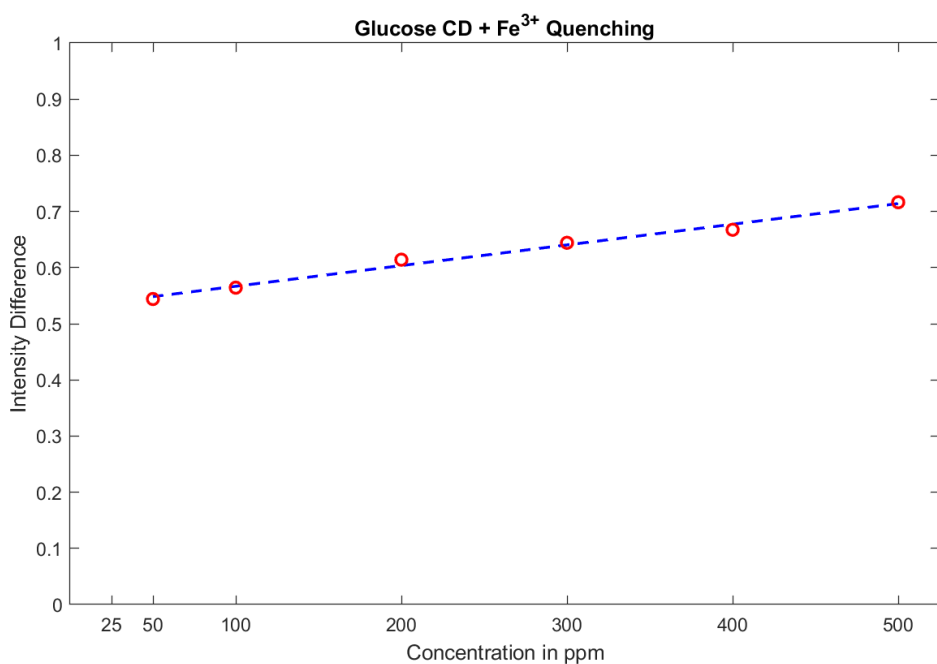


Figure 33: Calibration curve for Fe(III)-related quenching.

The slope of the curve gives information about the sensing sensitivity of the system. In the case of Cr(III) sensing, the slope equals to  $m = 0.0007$ , while for the Fe(III) case the slope is  $m = 0.0004$ .

This means that, even though conjugation with Fe(III) resulted in a far more quenched response even at low concentrations, the sensitivity of the system is better in the case of Cr(III) sensing. On the contrary, a better limit of detection (LoD) is obtained with Fe(III).

In order to understand the difference in quenched response between the two metals, crystal field theory (CFT) has to be addressed. CFT is related to bonds between ligands and transition metals, and describes the breaking of  $d$ -type orbital degeneracy for the latter. When a ligand approaches the metal, its field enters in contact with the electron orbitals of the metal that, due to electron-electron repulsion, split and shift to higher energies. The energy difference between the split orbitals equals to the crystal field splitting energy  $\Delta_o$ .

The chosen transition metals for this thesis work, Fe(III) and Cr(III), possess an octahedral molecular symmetry, meaning that they hold a coordination number of 6, thus ligands can bind around the metal centre in six places. The molecular symmetry of the metals dictates which  $d$ -type orbitals will shift to higher energies. A schematic of the octahedral symmetry is reported in Figure 34.

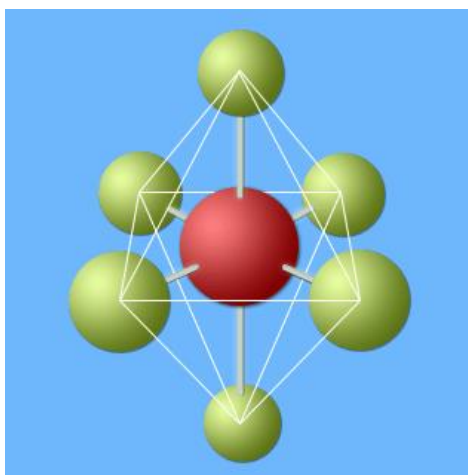


Figure 34: Octahedral molecular symmetry (Reproduced with Creative Commons license).

Furthermore, the orbital splitting for these metals occurs for the  $3d$  orbitals. When  $3d$  orbitals split due to the crystal field, in the case of octahedral symmetry, the  $d_{z^2}$  and  $d_{x^2-y^2}$  orbitals ( $e_g$ ) rise in energy, while the remaining  $d_{xy}$ ,  $d_{xz}$ ,  $d_{yz}$  ( $t_{2g}$ ) remain at lower energy. This behaviour is made explicit in Figure 35.

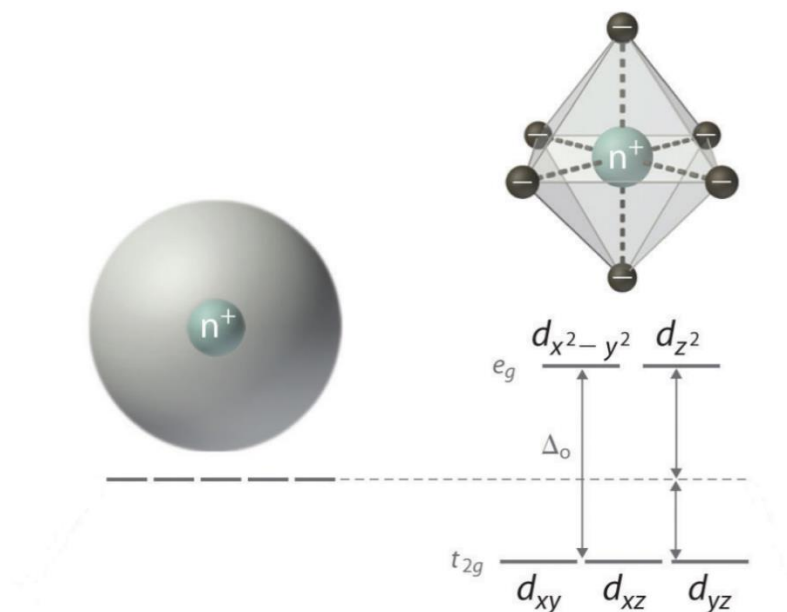


Figure 35: 3d orbitals splitting (Reproduced with Creative Commons license).

After the splitting, two spin configurations become possible, depending on the spin pairing energy  $P$  required by the electrons to occupy a specific orbital.

If the pairing energy is less than the crystal field splitting energy,  $P < \Delta_o$ , electrons will occupy lower energy orbitals, resulting in the so-called *low spin configuration*. On the contrary, if the pairing energy is higher,  $P > \Delta_o$ , electrons can occupy higher energy orbitals and the *high spin configuration* is obtained. In particular, Fe(III) assumes low spin configuration, while Cr(III) assumes the high spin one. The two spin configurations are depicted in Figure 36.

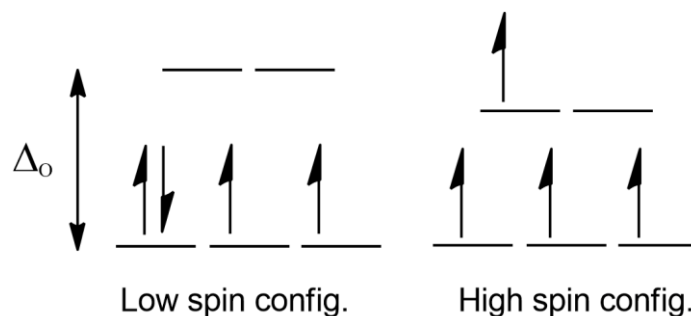


Figure 36: Low spin (left) and high spin (right) configurations.

Unfortunately, the exact nature of the resulting complex between the CDs and the metal is unknown and requires further studies. Nonetheless, some hypotheses can be made regarding the difference in quenching between the two metal ions.

The stronger quenching given by Fe(III) could be related to it assuming a low spin configuration. In complexation with the CDs, electrons from the dots migrating to the metal could position themselves in the lower energy orbitals, due to it being more energy convenient. This could result in the formation of an energetically lower ground state complex. Indeed, fluorescent emission intensity depends on

states distribution in the complex, thus the relative quenching effect is affected by the ground state of the complex, and could result in a lower emission intensity, meaning a stronger quenching effect.

The opposite could be true for Cr(III), meaning that the resulting complex could possess a higher energy with respect to the one formed with Fe(III) and thus a higher fluorescence, resulting in a weaker quenching effect.

Moreover, since low spin configuration is more energetically favourable, a higher number of electrons could migrate for the case of complexation between CDs and Fe(III) with respect to complexation with Cr(III), thus generating a higher number of metal-organic complexes which quench the fluorescence emission.

## 5 Conclusions

The thesis work focused on the use of carbon dots as fluorescent probes for the detection of harmful metals, namely Cr(III) and Fe(III), through the fluorescence quenching effect.

Glucose CDs with a CND structure were synthesised through hydrothermal method in an autoclave. Spectroscopic characterizations were performed and the fluorescence emission spectrum was registered. Both excitation-dependent and -independent bands were found, with the former chosen as the preferred band for the quenching application.

Metal containing solutions were prepared for each metal and conjugation with the CDs was performed by mixing CDs into the solutions. Fluorescence was again measured for the solutions containing the conjugation between CDs and metals. As expected, fluorescence intensity decreased, meaning that the quenching phenomenon given by the metal particles took place. The results were measurable even at low metal concentrations, namely 25 ppm.

By comparing the calibration curves extrapolated for the two metals, the system was found to be more sensitive to Cr(III) particles, while a greater quenching effect was measured for Fe(III) particles resulting in a greater limit of detection.

The results were satisfactory, since a decrease in fluorescence emission intensity was observed even at low metal concentrations and thus metal detection through the use of CDs was possible. Moreover, the emission related to Cr(III) conjugation was strongly concentration dependent, yielding not only qualitative information about the presence of the metal in the surroundings, but also quantitative.

Future developments could include an improvement in sensibility, achieved by acting on the hydrothermal synthesis parameters or by the inclusion of heteroatoms in the process. Moreover, the sensing could be extended to further harmful metals for humans such as arsenic, beryllium, cadmium, lead and mercury, or heavy metals commonly present in the waters such as zinc, copper, manganese and barium that are dangerous not only to humans but also to the marine environment. Furthermore, metal sensing could be performed for several sample matrices.

## Acknowledgements

First and foremost, I would like to thank Professor Alberto Tagliaferro for given me the opportunity to work alongside his research group. It was an incredibly fascinating experience that I will hold dear to my heart.

I would like to thank Dr. Mattia Bartoli for always assisting and guiding me during these months, giving me insights not only on an academic level but also human one. Thank you so much for your availability and patience.

I'm deeply grateful to my parents and my entire family, for never leaving my side and always encouraging and supporting me in my decisions. I love you all from the bottom of my heart.

I'm extremely grateful to Barbara, for assisting me and caring for me every second during this journey, since the first day. I'm very lucky to have you by my side.

Very heartfelt thanks to my colleague and partner in crime Danilo, with whom I shared joys, fears, deliriums, mana tapping and Lacrimosas. I'm proud and grateful to have shared this path with you.

I would like to thank my frog colleagues and most importantly curse-partners Angelo, Bruno, Davide, Enrico, Marco and Matteo.

My heartfelt thanks to the family that accompanied me during this second journey, the MPSG: Alessio, Antonio, Gianpaolo, Marco, Matteo, Vincenzo and my *figlioccio* Alessandro. I will keep your love and friendship in my heart forever.

Sincere thanks to the other family that accompanied me during my entire academic journey, the Priorato: Alessio, Davide, Manuel, Salvatore and Vito. These times with you shaped the person I am today.

Last but not least, many thanks to Antonio and Giovanni, which showed me love and support even from a distance. Plus Ultra.

## Bibliography

1. Lim, S.Y.; Shen, W.; Gao, Z. Carbon quantum dots and their applications. *Chemical Society Reviews* **2015**, *44*, 362-381.
2. Sanni, S.O.; Moundzounga, T.H.; Oseghe, E.O.; Haneklaus, N.H.; Viljoen, E.L.; Brink, H.G. One-Step Green Synthesis of Water-Soluble Fluorescent Carbon Dots and Its Application in the Detection of Cu<sup>2+</sup>. *Nanomaterials* **2022**, *12*, 958.
3. Liu, J.; Li, R.; Yang, B. Carbon dots: A new type of carbon-based nanomaterial with wide applications. *ACS Central Science* **2020**, *6*, 2179-2195.
4. Calabrese, G.; De Luca, G.; Nocito, G.; Rizzo, M.G.; Lombardo, S.P.; Chisari, G.; Forte, S.; Sciuto, E.L.; Conoci, S. Carbon dots: an innovative tool for drug delivery in brain tumors. *International Journal of Molecular Sciences* **2021**, *22*, 11783.
5. Zhao, C.; Song, X.; Liu, Y.; Fu, Y.; Ye, L.; Wang, N.; Wang, F.; Li, L.; Mohammadniaei, M.; Zhang, M. Synthesis of graphene quantum dots and their applications in drug delivery. *Journal of Nanobiotechnology* **2020**, *18*, 1-32.
6. Ross, S.; Wu, R.-S.; Wei, S.-C.; Ross, G.M.; Chang, H.-T. The analytical and biomedical applications of carbon dots and their future theranostic potential: A review. *Journal of Food and Drug Analysis* **2020**, *28*, 677.
7. Mishra, V.; Patil, A.; Thakur, S.; Kesharwani, P. Carbon dots: emerging theranostic nanoarchitectures. *Drug discovery today* **2018**, *23*, 1219-1232.
8. Hutton, G.A.; Martindale, B.C.; Reisner, E. Carbon dots as photosensitisers for solar-driven catalysis. *Chemical Society Reviews* **2017**, *46*, 6111-6123.
9. Chen, B.B.; Liu, M.L.; Huang, C.Z. Carbon dot-based composites for catalytic applications. *Green Chemistry* **2020**, *22*, 4034-4054.
10. Yu, J.; Song, H.; Li, X.; Tang, L.; Tang, Z.; Yang, B.; Lu, S. Computational studies on carbon dots electrocatalysis: a review. *Advanced Functional Materials* **2021**, *31*, 2107196.
11. Chen, J.; Xiao, G.; Duan, G.; Wu, Y.; Zhao, X.; Gong, X. Structural design of carbon dots/porous materials composites and their applications. *Chemical Engineering Journal* **2021**, *421*, 127743.
12. Lo Bello, G.; Bartoli, M.; Giorcelli, M.; Rovere, M.; Tagliaferro, A. A Review on the Use of Biochar Derived Carbon Quantum Dots Production for Sensing Applications. *Chemosensors* **2022**, *10*, 117.
13. Sun, X.; Lei, Y. Fluorescent carbon dots and their sensing applications. *TrAC Trends in Analytical Chemistry* **2017**, *89*, 163-180.
14. Xia, C.; Zhu, S.; Feng, T.; Yang, M.; Yang, B. Evolution and Synthesis of Carbon Dots: From Carbon Dots to Carbonized Polymer Dots. *Advanced Science* **2019**, *6*, 1901316, doi:<https://doi.org/10.1002/advs.201901316>
15. Tian, P.; Tang, L.; Teng, K.; Lau, S. Graphene quantum dots from chemistry to applications. *Materials today chemistry* **2018**, *10*, 221-258.
16. Permatasari, F., Aimon, A., Iskandar, F. et al. Role of C–N Configurations in the Photoluminescence of Graphene Quantum Dots Synthesized by a Hydrothermal Route. *Sci Rep* **6**, 21042 (2016). <https://doi.org/10.1038/srep21042>.
17. Rono, N.; Kibet, J.K.; Martincigh, B.S.; Nyamori, V.O. A review of the current status of graphitic carbon nitride. *Critical Reviews in Solid State and Materials Sciences* **2021**, *46*, 189-217.
18. Tao, S.; Zhu, S.; Feng, T.; Xia, C.; Song, Y.; Yang, B. The polymeric characteristics and photoluminescence mechanism in polymer carbon dots: A review. *Materials Today Chemistry* **2017**, *6*, 13-25, doi:<https://doi.org/10.1016/j.mtchem.2017.09.001>.
19. J. Phys. Chem. Lett. 2019, *10*, 17, 5182–5188, doi: <https://doi.org/10.1021/acs.jpcclett.9b01384>.
20. Zhou, Y.; Sharma, S.K.; Peng, Z.; Leblanc, R.M. Polymers in carbon dots: a review. *Polymers* **2017**, *9*, 67.
21. Zuo, P.; Lu, X.; Sun, Z.; Guo, Y.; He, H. A review on syntheses, properties, characterization and bioanalytical applications of fluorescent carbon dots. *Microchimica Acta* **2016**, *183*, 519-542.
22. Barman, M.K.; Patra, A. Current status and prospects on chemical structure driven photoluminescence behaviour of carbon dots. *Journal of Photochemistry and Photobiology C: Photochemistry Reviews* **2018**, *37*, 1-22.
23. Sobiech, M.; Luliński, P.; Wiecek, P.P.; Marć, M. Quantum and carbon dots conjugated molecularly imprinted polymers as advanced nanomaterials for selective recognition of analytes in environmental, food and biomedical applications. *TrAC Trends in Analytical Chemistry* **2021**, *142*, 116306.
24. Li, X.; Fu, Y.; Zhao, S.; Xiao, J.; Lan, M.; Wang, B.; Zhang, K.; Song, X.; Zeng, L. Metal ions-doped carbon dots: Synthesis, properties, and applications. *Chemical Engineering Journal* **2022**, *430*, 133101.

25. Hettiarachchi, S.D.; Graham, R.M.; Mintz, K.J.; Zhou, Y.; Vanni, S.; Peng, Z.; Leblanc, R.M. Triple conjugated carbon dots as a nano-drug delivery model for glioblastoma brain tumors. *Nanoscale* **2019**, *11*, 6192-6205.
26. Freire, R.; Le, N.D.; Jiang, Z.; Kim, C.S.; Rotello, V.M.; Fecine, P. NH<sub>2</sub>-rich Carbon Quantum Dots: A protein-responsive probe for detection and identification. *Sensors and Actuators B: Chemical* **2018**, *255*, 2725-2732.
27. Hill, S.A.; Benito-Alifonso, D.; Davis, S.A.; Morgan, D.J.; Berry, M.; Galan, M.C. Practical three-minute synthesis of acid-coated fluorescent carbon dots with tuneable core structure. *Scientific Reports* **2018**, *8*, 1-10.
28. Xu, X.; Ray, R.; Gu, Y.; Ploehn, H.J.; Gearheart, L.; Raker, K.; Scrivens, W.A. Electrophoretic analysis and purification of fluorescent single-walled carbon nanotube fragments. *Journal of the American Chemical Society* **2004**, *126*, 12736-12737.
29. Zhou, S.; Sui, Y.; Zhu, X.; Sun, X.; Zhuo, S.; Li, H. Study and Comparison on Purification Methods of Multicolor Emission Carbon Dots. *Chemistry – An Asian Journal* **2021**, *16*, 348-354, doi:<https://doi.org/10.1002/asia.202001352>.
30. Zhou, Y.; Liyanage, P.Y.; Geleroff, D.L.; Peng, Z.; Mintz, K.J.; Hettiarachchi, S.D.; Pandey, R.R.; Chusuei, C.C.; Blackwelder, P.L.; Leblanc, R.M. Photoluminescent Carbon Dots: A Mixture of Heterogeneous Fractions. *ChemPhysChem* **2018**, *19*, 2589-2597, doi:<https://doi.org/10.1002/cphc.201800248>.
31. Yan, F.; Sun, Z.; Zhang, H.; Sun, X.; Jiang, Y.; Bai, Z. The fluorescence mechanism of carbon dots, and methods for tuning their emission color: a review. *Microchimica Acta* **2019**, *186*, 583, doi:10.1007/s00604-019-3688-y.
32. Liu, M. Optical Properties of Carbon Dots: A Review. *Nanoarchitectonics*, Volume 1, Issue 1, **2020**, doi:<https://doi.org/10.37256/nat.112020124.1-12>.
33. Sarkar, Sunandan, et al. "Graphitic nitrogen doping in carbon dots causes red-shifted absorption." *The Journal of Physical Chemistry C* **120.2** (2016): 1303-1308.
34. Bao, Lei, et al. "Electrochemical tuning of luminescent carbon nanodots: from preparation to luminescence mechanism." *Advanced materials* **23.48** (2011): 5801-5806.
35. Connerade, J.P. A review of quantum confinement. In *Proceedings of the AIP Conference Proceedings*, 2009; pp. 1-33.
36. Zhu, S.; Song, Y.; Zhao, X.; Shao, J.; Zhang, J.; Yang, B. The photoluminescence mechanism in carbon dots (graphene quantum dots, carbon nanodots, and polymer dots): current state and future perspective. *Nano research* **2015**, *8*, 355-381.
37. Yan, F.; Sun, Z.; Zhang, H.; Sun, X.; Jiang, Y.; Bai, Z. The fluorescence mechanism of carbon dots, and methods for tuning their emission color: a review. *Microchimica Acta* **2019**, *186*, 583, doi:10.1007/s00604-019-3688-y.
38. Yu, J.; Liu, C.; Yuan, K.; Lu, Z.; Cheng, Y.; Li, L.; Zhang, X.; Jin, P.; Meng, F.; Liu, H. Luminescence Mechanism of Carbon Dots by Tailoring Functional Groups for Sensing Fe<sup>3+</sup> Ions. *Nanomaterials* **2018**, *8*, 233.
39. Sachdev, A.; Matai, I.; Gopinath, P. Implications of surface passivation on physicochemical and bioimaging properties of carbon dots. *RSC advances* **2014**, *4*, 20915-20921.
40. Zhu, S.; Song, Y.; Shao, J.; Zhao, X.; Yang, B. Non-conjugated polymer dots with crosslink-enhanced emission in the absence of fluorophore units. *Angewandte Chemie International Edition* **2015**, *54*, 14626-14637.
41. Liu, S.G.; Luo, D.; Li, N.; Zhang, W.; Lei, J.L.; Li, N.B.; Luo, H.Q. Water-soluble nonconjugated polymer nanoparticles with strong fluorescence emission for selective and sensitive detection of nitro-explosive picric acid in aqueous medium. *ACS Applied Materials & Interfaces* **2016**, *8*, 21700-21709.
42. Lee, H.; Su, Y.-C.; Tang, H.-H.; Lee, Y.-S.; Lee, J.-Y.; Hu, C.-C.; Chiu, T.-C. One-pot hydrothermal synthesis of carbon dots as fluorescent probes for the determination of mercuric and hypochlorite ions. *Nanomaterials* **2021**, *11*, 1831.
43. Rajendran, S.; Ramanaiah, D.V.; Kundu, S.; Bhunia, S.K. Yellow Fluorescent Carbon Dots for Selective Recognition of As<sup>3+</sup> and Fe<sup>3+</sup> Ions. *ACS Applied Nano Materials* **2021**, *4*, 10931-10942.
44. Wang, L.; Jana, J.; Chung, J.S.; Hur, S.H. Glutathione modified N-doped carbon dots for sensitive and selective dopamine detection. *Dyes and Pigments* **2021**, *186*, 109028.
45. Fu, Y.; Huang, L.; Zhao, S.; Xing, X.; Lan, M.; Song, X. A carbon dot-based fluorometric probe for oxytetracycline detection utilizing a Förster resonance energy transfer mechanism. *Spectrochimica Acta Part A: Molecular and Biomolecular Spectroscopy* **2021**, *246*, 118947.
46. Zhang, H.; Liu, J.; Wang, B.; Liu, K.; Chen, G.; Yu, X.; Li, J.; Yu, J. Zeolite-confined carbon dots: tuning thermally activated delayed fluorescence emission via energy transfer. *Materials Chemistry Frontiers* **2020**, *4*, 1404-1410.
47. Li, G.; Fu, H.; Chen, X.; Gong, P.; Chen, G.; Xia, L.; Wang, H.; You, J.; Wu, Y. Facile and sensitive fluorescence sensing of alkaline phosphatase activity with photoluminescent carbon dots based on inner filter effect. *Analytical chemistry* **2016**, *88*, 2720-2726.

48. Liu, S.; Zhao, N.; Cheng, Z.; Liu, H. Amino-functionalized green fluorescent carbon dots as surface energy transfer biosensors for hyaluronidase. *Nanoscale* **2015**, *7*, 6836-6842.
49. Lin, Z.; Xue, W.; Chen, H.; Lin, J.-M. Classical oxidant induced chemiluminescence of fluorescent carbon dots. *Chemical Communications* **2012**, *48*, 1051-1053, doi:10.1039/C1CC15290D.
50. Xu, Y.; Wu, M.; Feng, X.Z.; Yin, X.B.; He, X.W.; Zhang, Y.K. Reduced carbon dots versus oxidized carbon dots: photo-and electrochemiluminescence investigations for selected applications. *Chemistry—A European Journal* **2013**, *19*, 6282-6288.
51. Lerf, A.; He, H.; Forster, M.; Klinowski, J. Structure of graphite oxide revisited. *The Journal of Physical Chemistry B* **1998**, *102*, 4477-4482.
52. Wiśniewski, M. The Consequences of Water Interactions with Nitrogen-Containing Carbonaceous Quantum Dots—The Mechanistic Studies. *International Journal of Molecular Sciences* **2022**, *23*, 14292.
53. Mintz, K.J.; Bartoli, M.; Rovere, M.; Zhou, Y.; Hettiarachchi, S.D.; Paudyal, S.; Chen, J.; Domena, J.B.; Liyanage, P.Y.; Sampson, R.; et al. A deep investigation into the structure of carbon dots. *Carbon* **2021**, *173*, 433-447, doi:<https://doi.org/10.1016/j.carbon.2020.11.017>.
54. Seven, E.S.; Kirbas Cilingir, E.; Bartoli, M.; Zhou, Y.; Sampson, R.; Shi, W.; Peng, Z.; Ram Pandey, R.; Chusuei, C.C.; Tagliaferro, A.; et al. Hydrothermal vs microwave nanoarchitectonics of carbon dots significantly affects the structure, physicochemical properties, and anti-cancer activity against a specific neuroblastoma cell line. *Journal of Colloid and Interface Science* **2023**, *630*, 306-321, doi:<https://doi.org/10.1016/j.jcis.2022.10.010>.
55. Liu, M.; Chen, B.; Li, C.; Huang, C. Carbon dots: synthesis, formation mechanism, fluorescence origin and sensing applications. *Green Chem.*, 2019, **2021**, 449, doi:10.1039/c8gc02736f.
56. Shen J, Zhu Y, Yang X, Li C. Graphene quantum dots: emergent nanolights for bioimaging, sensors, catalysis and photovoltaic devices. *Chem. Commun. (Camb.)*, **2012**, *48*(31): 3686–3699.
57. S. Kim, S. W. Hwang, M. K. Kim, Y. S. Dong, H. S. Dong, O. K. Chang, S. B. Yang, J. H. Park, E. Hwang, S. H. Choi, G. Ko, S. Sim, C. Sone, H. J. Choi, S. Bae and B. H. Hong, *ACS Nano*, **2012**, *6*, 8203–8208.
58. H. Ding, S. B. Yu, J. S. Wei and H. M. Xiong, *ACS Nano*, **2016**, *10*, 484–491.
59. Zanyar Movasaghi, Shazza Rehman & Dr. Ihtesham ur Rehman (2008) *Fourier Transform Infrared (FTIR) Spectroscopy of Biological Tissues*, *Applied Spectroscopy Reviews*, *43:2*, 134-179, doi:10.1080/05704920701829043.
60. Hou, Di-Bo & Zhang, Jian & Chen, Lin & Huang, Ping-Jie & Zhang, Guang-Xin. (2013). *Water Quality Analysis by UV-Vis Spectroscopy: A Review of Methodology and Application*. *Guang pu xue yu guang pu fen xi = Guang pu*. *33*. 1839-44. 10.3964/j.issn.1000-0593(2013)07-1839-06.
61. *RSC Adv.*, 2013,**3**, 8286-8290.
62. Nguyen, H. Y.; Le, X. H.; Dao, N. T.; Pham, N. T.; Vu, T. H. H.; Nguyen, N. H.; Pham, T. N. *Microwave-assisted synthesis of graphene quantum dots and nitrogen-doped graphene quantum dots: Raman characterization and their optical properties*, *Advances in Natural Sciences: Nanoscience and Nanotechnology*, Volume 10, Issue 2, id.025005, doi: 10.1088/2043-6254/ab1b73.